# PREPARATION OF METEOROLOGICAL FIELDS FOR THE SEPTEMBER 21-24, 1997 SOUTHERN CALIFORNIA OZONE STUDY (SCOS) EPISODE USING THE MM5 PROGNOSTIC MODEL

**Final Report**
**Contract No. 00-719**

**by**

**Nelson L. Seaman, P.I.**
**David R. Stauffer, Co-P.I.**
**Glenn K. Hunter**

**Department of Meteorology**
**The Pennsylvania State University**
**University Park, PA 16802**

**and**

**Neil J. M. Wheeler, Co-P.I.**

**Sonoma Technology, Inc.**
**1360 Redwood Way, Suite C**
**Petaluma, CA 94954**

**Prepared for the California Air Resources Board**

**10th and I Streets**
**Sacramento, CA 95814**

**1 November 2003**

## Disclaimer

The statements and conclusions in the Report are those of the contractor and not necessarily those of the California Air Resources Board. The mention of commercial products, their source, or their use in connection with material reported herein is not to be construed as actual or implied endorsement of such products.

## Acknowledgements

This report was submitted in fulfillment of the California Air Resources Board Contract No. 00-719, titled "Preparation of Meteorological Fields for the September 21-24, 1997, Southern California Ozone Study (SCOS) Episode Using the MM5 Prognostic Model", by The Pennsylvania State University and Sonoma Technology, Inc. under the sponsorship of the California Air Resources Board. Work was completed on 31 March 2003. We gratefully acknowledge that special SCOS-97 data sets were supplied to the contractors by the California Air Resources Board.

## Table of Contents

## List of Figures

## List of Tables

## Abstract

The SCOS-97 September 21-25 episode was dominated by the passage of an upper-level ridge on 22-23 September, 1997, followed by the approach of a tropical storm moving northward from Baja CA. These events caused mid-level winds to shift from northwesterly to southeasterly over the SoCAB and the border areas near Mexico, resulting in a weak, near-stagnant surface conditions in the SoCAB near the middle of the episode and elevated levels of ozone. Light southeasterly winds on 23 September caused heavily polluted air to be transported west-northwest from Los Angeles to Ventura and Santa Barbara counties. Later, the tropical storm caused southeasterly winds to intensify so that ozone levels dropped dramatically as the episode came to an end on 24 September.

The non-hydrostatic MM5 mesoscale meteorological model was applied to the 21-25 September 1997 SCOS episode with three nested-grid domains having horizontal meshes of 45 km, 15 km and 5 km. The inner domain covered the SoCAB region and extended far enough southward and eastward to include the border areas of Mexico. The model had 45 layers in the vertical to allow relatively fine resolution up to about 3 km to better simulate deep mixing layers over the southeastern CA deserts. Five experiments were run, using different strategies for data assimilation and lower boundary conditions. The most successful experiment (Exp. 3) used modified (warmer) lower boundary conditions, plus both obs-nudging and analysis nudging. The resulting model solutions had domain-averaged RMS errors for surface-layer wind speed of 1.78 $ms^{-1}$. Because the average wind speed was very slow in the coastal air basins, where most of the observation sites are located, the MAE for surface-layer wind-direction error in Exp. 3 was 51 degrees. However, these direction errors appear to be more related to surface irregularities in light-wind conditions than to serious systematic model errors. Boundary-layer wind direction errors were only ~27 degrees. Moreover, Experiment 3 did fairly well in capturing the shift of wind directions that occurred as the upper-level ridge passed over the SoCAB and the later effects due to the approach of the tropical storm from the south. A final Experiment 4, using a technique developed under ARB funding for assimilating surface temperature and mixing ratios further decreased errors in these two thermodynamic fields, although some biases toward cool and moist conditions remained.

## Executive Summary

The non-hydrostatic MM5 mesoscale meteorological model was applied to the 21-25 September 1997 SCOS episode with three-nested grid domains having horizontal meshes of 45 km, 15 km and 5 km. The inner domain covered the SoCAB region and was extended far enough southward and eastward to include the border areas of Mexico. The model had 45 layers in the vertical to allow relatively fine resolution up to about 3 km to better simulate deep mixing layers over the southeastern CA deserts.

The SCOS-97 September 21-25 episode was dominated by the passage of an upper-level ridge on 22-23 September that caused mid-level winds to shift from northwesterly to southeasterly over the SoCAB and the border areas near Mexico. As a result of the ridge passage, northwesterly winds from the Pacific Ocean were weakened and airflow in the SoCAB stagnated, leading to elevated levels of ozone. The southeasterly winds became slightly stronger on 23 September, which caused heavily polluted air to be transported west-northwest from Los Angeles to Ventura and Santa Barbara counties, where brief local exceedances of the 1-h ozone standard were approached. At the same time temperatures rose several degrees C in the coastal basins due to reduced advection of cool marine air, plus the westward advection of warm air from the southeastern CA deserts. During the second half of the episode a tropical storm that had been slowly progressing northward from the southern tip of the Baja Peninsula began to affect the SoCAB and border areas. The tropical storm caused southeasterly winds to intensify and by 24 September, subtropical moist air penetrated into the SoCAB. The increasing winds and clouds prevented active photochemistry and caused airborne chemical species to be advected rapidly out of the region, so that ozone levels dropped dramatically as the episode came to an end on 24 September.

The following are the main conclusions from the numerical experiments conducted for this case:

- The Control Experiment 1 for the SCOS-97 September 21-25 episode was successful inasmuch as no large systematic errors developed in the winds that would suggest serious imbalances in the dynamical forcing of the MM5 model. However, there were serious cold biases on the order of 4 C in the model solutions that did affect adversely the intensity of the sea breeze circulation and precluded the development of nocturnal land breezes. Thus, the model's thermodynamic errors along the coast could have moderately negative impacts on the advection of pollutants in and from the coastal air basins during the early and middle parts of the episode, before the influence of the tropical storm began to dominate the SoCAB.

- Using only standard analysis nudging Experiment 2 significantly reduced errors in the wind speed, but did not have much impact on the temperature or wind direction errors. Temperatures on average remained too cool by about 4 C. The cause of the cool temperatures was diagnosed to be due to a combination of two factors. First, NASA 9-km resolution sea-surface temperature images indicated that the NCEP sea-surface temperature analysis was too cool by 2-6 C over much of the CA Bight. Second, default values for the MM5's deep-soil temperatures were quite likely too

cool for this late-September episode, which falls around the time of maximum deep-soil temperatures expected near the end of summer.

- Experiment 2.5 tested the hypothesis that erroneously cool land and sea-surface temperature specifications caused MM5's air-temperature simulations to average ~4 C too cold in Experiments 1 and 2. The deep soil temperature was raised to 4 C above the climatological average and NCEP sea-surface temperatures were replaced by NASA sea temperatures observed at 9-km resolution. This experiment included the analysis nudging used in Exp. 2. Results showed dramatic improvement in the MM5-simulated temperature field, with MAE dropping from ~4.4 C to 2.8 C. However, because of the warmer ocean temperatures, mixing ratio also rose, introducing a low-level moist bias of ~ 3 $gkg^{-1}$. More important from an air-quality perspective, the changes made to the lower boundary conditions allowed the model to simulate a weak offshore-directed land breeze during the hours near sunrise. This change in the winds was confirmed by a number of 1200 UTC observations on the morning of 22 September.

- Experiment 3 used the modified lower boundary conditions, plus both obs-nudging and analysis nudging. The resulting model solutions had domain-averaged RMS errors for surface-layer wind speed of 1.78 $ms^{-1}$. Because the average wind speed was very slow in the coastal air basins, where most of the observation sites are located, the MAE for surface-layer wind-direction error in Exp. 3 was 51 degrees. However, these direction errors appear to be more related mostly to the influence of surface irregularities (trees, buildings, hills, etc.) in light-wind conditions than to serious systematic model errors. Also, the very light mean winds caused the normalized wind speed errors to appear relatively large. In the layer from 25-1500 m AGL, where small surface irregularities have less effect, the MAE for direction dropped to 27 degrees, with an RMS error of wind speed = 1.60 $ms^{-1}$. On the other hand, despite the improvement of the lower-boundary conditions, the MAE for surface temperature remained somewhat larger than desired, $MAE_T$ = 2.73 C. Overall, this experiment produced the best match to observations of the standard FDDA approaches. Moreover, Experiment 3 did fairly well in capturing the shift of wind directions that occurred as the upper-level ridge passed over the SoCAB and the acceleration of southeast winds on 24 September due to the approach of the tropical storm from the south.

- Experiment 4 extended Exp. 3 by adding the method developed by Alapaty et al. (2001) for assimilating surface temperature and mixing ratio data. This experiment was only moderately successful. The MAE for surface temperature on the 5-km domain was decreased further to 2.53 C (larger corrections occurred at times of the day when model errors had been greatest) and mixing ratio errors were lower (MAE = 2.15 g $kg^{-1}$). The wind statistics were virtually unchanged relative to Exp. 3. Thus, results of Exp. 4 were also quite successful, producing the best low-level temperature and moisture solutions, and therefore should be suitable for air-quality modeling applications.

The 21-25 September 1997 episode revealed that the methods for defining the lower boundary conditions in the MM5 over southern CA should be re-evaluated. The default method for estimating deep-soil temperatures and soil moisture tends to have significant biases. A more physically realistic land-surface model might be a valuable addition to the representation of the thermal and moisture processes in the MM5. Work on this topic has been underway in the MM5 community for some time. NCAR has installed a new five-layer land surface scheme that allows soil moisture content to vary with time. At the time that the present SCOS-97 modeling study was begun, the methodology for initializing soil moisture for the new land surface scheme was not yet mature enough to ensure accurate results, especially for the complex conditions in the LA Basin and its surroundings. However, recent advancements have introduced an upgraded version of the scheme that can be initialized with improved estimates of soil temperature and moisture produced by a similar land-surface model (LSM) run by NCEP. It is recommended that this new community land-surface model (called NOAH) should be tested and evaluated specifically for the SoCAB environment. It is possible that this LSM, in combination with improved satellite-measured sea-surface temperatures as used in the present study, could provide significant improvements for simulating the thermodynamics of the SoCAB.

# 1. INTRODUCTION

## 1.1 Background

The South Coast Air Basin (SoCAB) has been a prime focal area for photochemical modeling studies for many years because of the severe air pollution events it is subjected to from time to time. It is well known that the region's orography and Mediterranean climate combine with its large population and extensive anthropogenic emissions (from industrial, commercial, on-road and off-road vehicles, etc.) to produce and trap primary and secondary airborne chemical species in various airsheds. However, the very complex terrain and meteorology of the region make this an exceptionally difficult area in which to perform numerical modeling studies. Under such conditions both traditional prognostic meteorological models and diagnostic wind models often can produce data sets with fairly large errors or inconsistencies. In view of these challenges, advanced numerical techniques that combine dynamical modeling and observational databases generally provide the best method available for generating meteorological fields having fine resolution and 3-D inter-variable consistency (Seaman 2000).

In summer and early autumn 1997, the Air Resources Board (ARB) conducted the Southern California Ozone Study (SCOS-97) to gain a better air-quality and meteorological observational database for understanding poor air quality in the South Coast Air Basin (SoCAB). In addition to air chemistry data, special meteorological data were collected using radar wind profilers and a large number of surface meteorological sensors throughout southern CA. These data underwent preliminary quality control prior to being archived under ARB support.

An initial round of numerical modeling studies using certain of these meteorological data was conducted under an ARB sponsored project (Contract No. 97-310) aimed at evaluating and improving the accuracy of the Penn State/NCAR mesoscale meteorological model, MM5, for applications in CA. A focus of this prior numerical modeling was to improve the land-surface specifications and other aspects of the MM5 to better simulate meteorological conditions associated with poor air quality in the SoCAB during summer. Two SCOS-97 episodes were simulated and evaluated as part of that study: 4-7 August and 26-30 September 1997. The first of these episodes represented fairly typical SoCAB cases with poor air quality, with light to moderate sea breezes and little influence of clouds or fog over land. The second episode represented a more unusual case in that an upper-level low formed south of the SoCAB, first inducing clouds and showers over the SoCAB mountain ranges, followed by warm Santa Ana winds that dissipated the clouds and marine stratus. During the latter half of the 26-30 September case, the Santa Ana winds decayed as the upper-level cyclone weakened and coastal and marine stratus returned to the SoCAB and the Southern CA Bight.

The numerical modeling for the former study was conducted jointly by San Jose State University and the Pennsylvania State University. In consultation with scientists of the ARB, the resolution (mesh size) for the innermost model domain over the SoCAB was set at 5 km and the domain area extended from above Point Conception (~35.5 N) southward to about 40 km below the Mexican border (~32 N) (**Figure 1**). Special data from the SCOS-97 field program were assimilated into the MM5 numerical experiments using four-dimensional data assimilation

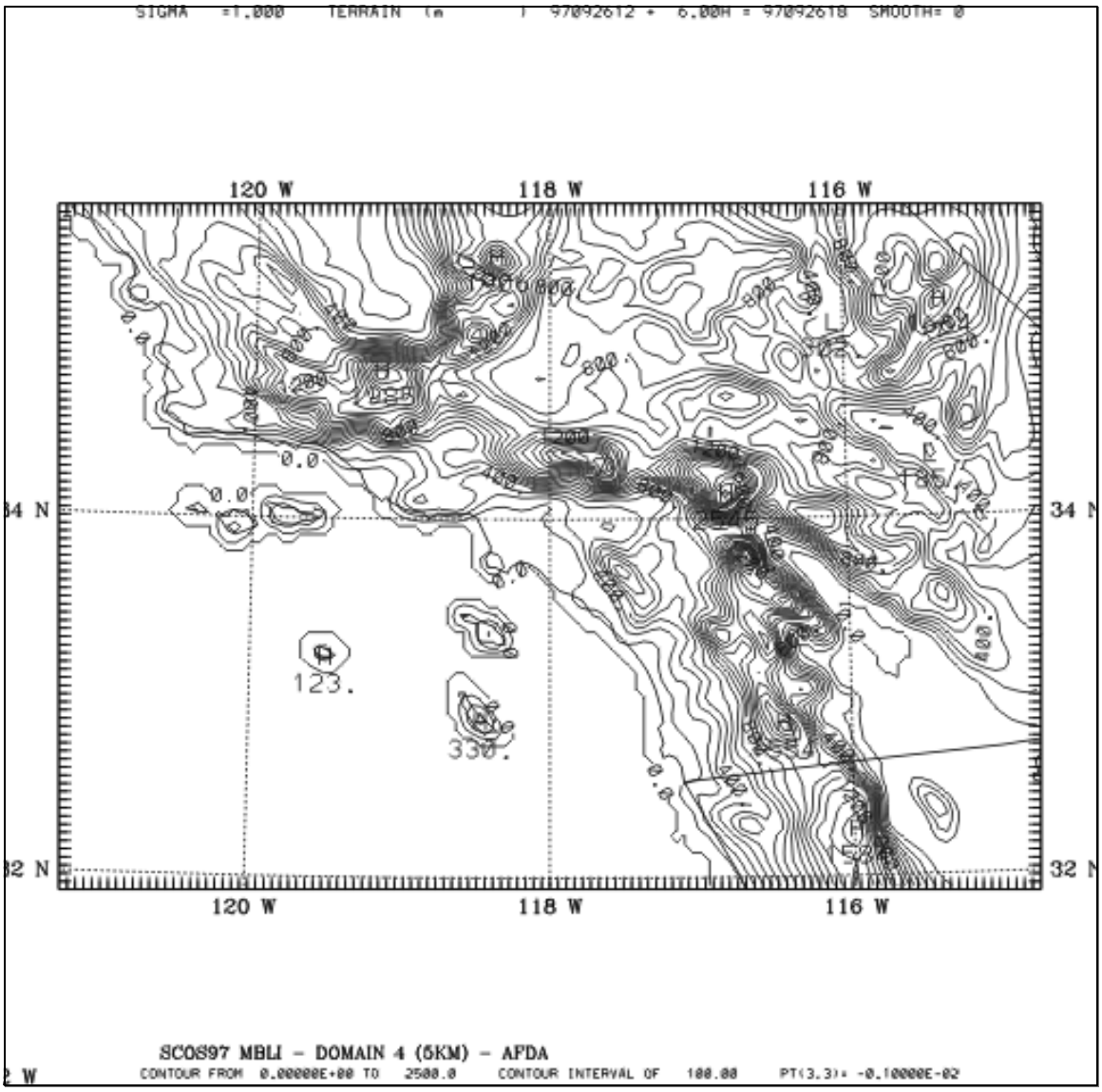


**Figure 1.** Terrain (m) on the innermost 5-km domain of the MM5 nested mesoscale model for the former project supported by ARB Contract No. 97-310 . Contour interval is 100 m.

(FDDA), as described by Stauffer and Seaman (1994) and Seaman et al. (1995). Results of this former SCOS-97 modeling study under Contract 97-310 have been provided in the project final report to ARB (Bornstein et al. 2001).

The modeling results of the more typical August episode were found to be generally accurate, while the results for the far more complex September case were somewhat mixed, with both good and less favorable aspects found in the solutions. The most serious difficulty in the model solutions for the 26-30 September episode was that the simulated Santa Ana winds became too intense during the height of the storm and extended too far over the CA Bight. Nevertheless, after 78 h of model run-time, MM5 correctly generated the redevelopment of coastal fog and marine stratus over the Pacific Ocean and light winds in the SoCAB following the end of the Santa Ana. The model produced realistic patterns of low-level fog and stratus with low liquid-water contents (mostly less than 0.5 g $kg^{-1}$) corresponding to the filmy fog/cloud patterns observed by the GOES-9 satellite (shallow depths and low-water content) (**Figures 2 and 3**).

### 1.2 Objectives of the Study

Previous ARB studies suggest that in certain events significant transport of air pollution occurs across the border with Mexico, in addition to the pollution generated locally in the SoCAB. Despite the mostly encouraging results from the previous SCOS-97 MM5 modeling study completed by Penn State and SJSU, ARB concluded that the 5-km domain in **Figure 1** did not extend far enough southward and eastward to allow reliable representation of cross-border flows. Therefore, the ***objective*** of the current study is ***to generate 3-D meteorological fields suitable for use in air-quality modeling studies for the period of 21-24 September 1997 over a domain that includes the South Coast air basins and extending southward to Ensenada, Mexico and eastward into Arizona.*** For this effort, the Penn State/NCAR mesoscale model, MM5 version 3.5 (see Section 2.1), was the basis for the development of the meteorological fields (that is, the current public-release version of the MM5 at the time the project was begun, updated from the original form described by Grell et al. 1994). The modeling design incorporates and builds on what was learned from the previous modeling experiments in the region (Bornstein et al. 2001).

Implied within the main ARB objective are several additional goals that are central to the success of the modeling effort. These goals involve accurate representation of the physical and dynamical features most critical to the transport, diffusion, and photochemistry of trace constituent species in the atmosphere, including the following:

- Mixing depth patterns evolving in space and time
- Vertical transport over complex heated topography
- Flow re-circulation above the boundary layer over complex terrain
- Sea/land breezes and mountain/valley winds
- Influence and distribution of clouds, coastal fog and precipitation over semi-arid subtropical regions, especially Baja California

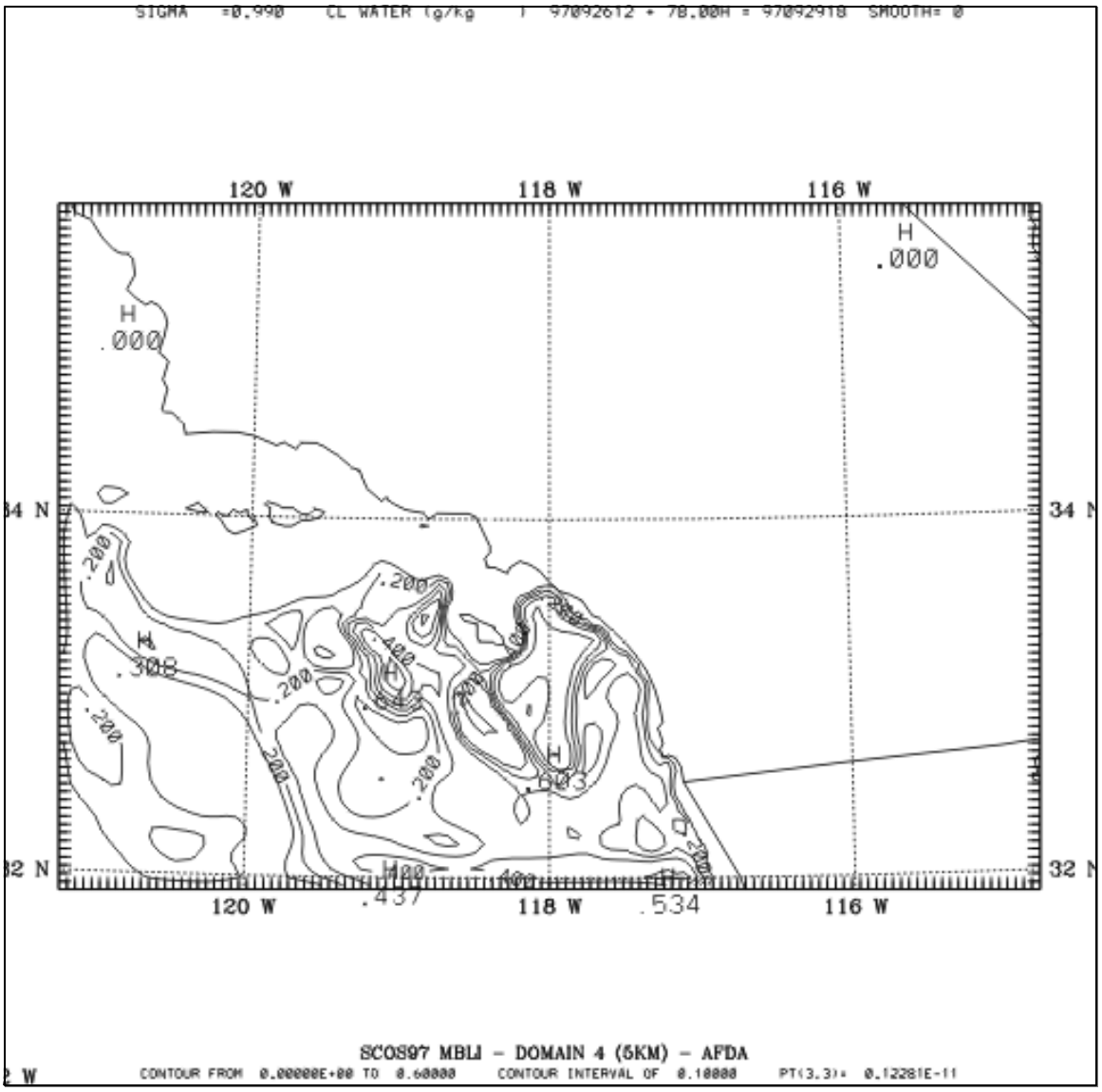


**Figure 2.** MM5 simulated cloud liquid water (g $kg^{-1}$) in the low levels at about 120 m AGL ($s$ = 0.990) for 1800 UTC, 29 September 1997, after 78 h of model integration. Contour interval is 0.1 g $kg^{-1}$. This modeling work was conducted under ARB Contract No. 97-310.

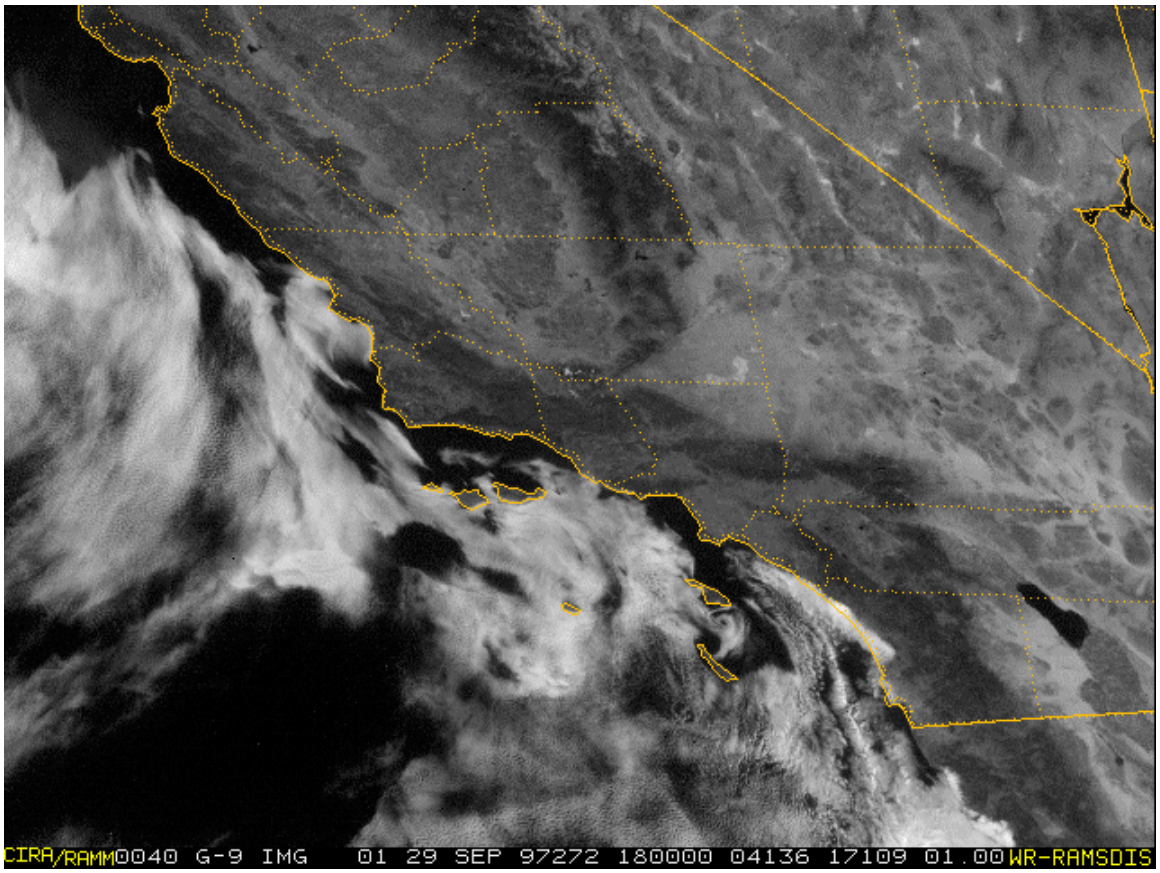


**Figure 3.** GOES-9 visible image at 1800 UTC, 29 September 1997.

In support of these goals, the ARB has worked cooperatively with the U.S. Environmental Protection Agency, the San Diego and Imperial Counties Air Pollution Control Districts, and Mexico's environmental agency, the Secretaria de Medio Ambiente, Recursos Naturales y Pesca, to address concerns about the air quality in the California-Baja California border region. The SCOS-97 observing systems were not specifically designed to include northern Mexico, although they did include a few sites as far south as the San Diego Air Basin. Consequently, to address questions related to cross-border air-quality, ARB has requested MM5 meteorological-modeling assistance for an additional episode from the SCOS-97 period. To allow study of the border region, in addition to the SoCAB, the boundaries of the highest-resolution model domain have been extended southward and eastward to include all of San Diego and Imperial Counties and ~100-km of northernmost Baja California from the border south to Ensenada (Section 2.3).

### 1.3 Organization of the Report

The organization of the final report begins with documentation of the features of the MM5 model and its data assimilation system that are important to the current study (Section 2). Next, Section 3 explains data quality control and the design of the numerical experiments, while Section 4 gives an overview of the air quality and meteorology in the 21-24 September 1997 episode. Results and discussion of the numerical runs appear in Section 5. Finally, Section 6 provides a summary of the most important findings and suggestions for future research that could build on the value of the present study.

## 2. THE METEOROLOGICAL MODELING SYSTEM

### 2.1 The PSU/NCAR MM5 Model

The model used for this study is the non-hydrostatic 3-D PSU/NCAR mesoscale model (Dudhia 1993), widely known as the MM5, version 3.5. This model and its pre- and post-processors have been described in detail by Grell et al. (1994) and Haagenson et al. (1994). Since the model is well-documented elsewhere, only an abbreviated description is provided here.

Briefly, the model uses the terrain-following "$s$" vertical coordinate (non-dimensionalized pressure) and a split semi-implicit temporal integration scheme. The terrain following vertical coordinate is an advantage for applications in areas having steep terrain, such as are common in California. The split-semi-implicit time integration is used in MM5 to provide relatively long time steps for advective terms [usually the time step, $\Delta t$, is set to $3 * \Delta x(km)$]. Meanwhile, those terms of the primitive equations responsible for the propagation of sound waves and fast gravity waves are treated with much shorter time steps. Prognostic primitive equations are used to predict the three wind components ($u$, $v$, and $w$), temperature ($T$), water vapor mixing ratio ($q_v$) and perturbation pressure ($p'$) in three dimensions. The perturbation pressure is the departure from a temporally invariant and hydrostatically balanced reference-state pressure ($p^*$), so that the total pressure at any location on the 3-D grid is given by $p(x,y,s,t) = p^*(x,y,s) + p'(x,y,s,t)$. Use of the constant reference-state pressure increases

the accuracy of gradient calculations in the vicinity of steep terrain and ensures that the location of the $s$ levels does not change during the model integration.

Users of the MM5 can define up to 10 different nested-grid domains at a time, with a 3:1 mesh ratio between successive nested grids. Otherwise, the horizontal and vertical resolutions of the model are arbitrary. The exchange of information between domains and the grid interfaces can be chosen to be either one-way or two-way interactive.

In this study, turbulent processes and mixed-layer depth are represented using a type of Mellor-Yamada (1974) 1.5-order parameterization. Known in MM5 as the Gayno-Seaman turbulence parameterization, it explicitly predicts the 3-D field of turbulent kinetic energy (TKE) (Gayno 1994, Shafran et al. 2000). Eddy diffusivity is diagnosed from the local TKE, while the boundary layer depth is diagnosed from the vertical profile of the TKE. A force-restore prognostic surface energy budget equation is used to predict the ground temperature ($T_g$) (Zhang and Anthes 1982). The surface physical properties (albedo, roughness length, moisture availability, emissivity and thermal inertia) are defined as a function of land use for 24 categories via a standard MM5 look-up table (modified for CA and northern Mexico).

Other important physical processes include precipitation and radiation. Resolved-scale precipitation is represented using the microphysics parameterization described by Dudhia (1989), which has explicit prognostic equations for suspended cloud water or cloud ice ($q_c$) and for rain water or snow ($q_r$). In the Dudhia precipitation scheme, there are no mixed-phase precipitation or cloud states and freezing occurs at an arbitrary temperature (defined here as 0 C). Convective precipitation is represented using the Kain-Fritsch (1990) cumulus parameterization. Finally, the effects of long-wave and short-wave radiation at the surface and at all levels in a column (including cloud effects on radiation) are treated with a single broad-band two-stream radiation parameterization (Dudhia 1989).

The code of the MM5 is written in Fortran 90 and Fortran 77. Its structure is highly modularized, so that physical parameterizations can be exchanged easily. All of the parameterizations discussed above are found in the official supported public-release version of the MM5 (available through NCAR's Mesoscale and Microscale Meteorology Division). Several options exist in the MM5 for each type of parameterization. The model is easily ported to a variety supercomputers, workstations and PCs, and a parallelized version of the code is available for use on distributed-memory massively parallelized computers.

## 2.2 The FDDA System

### 2.2.1 Standard FDDA

The four-dimensional data assimilation (FDDA) technique used in this study is based on the Newtonian relaxation approach, or nudging, described by Stauffer and Seaman (1990) and Seaman et al. (1995). Nudging is a continuous form of FDDA that relaxes the model state toward the observed state by adding to one or more of the prognostic equations artificial tendency terms based on the difference between the two states. It is said to be continuous

because the nudging term is applied at every time step, thereby minimizing "shock" to the model solutions that may occur in intermittent assimilation schemes. In this study both the analysis nudging approach described by Stauffer and Seaman (1990) and modified by Shafran et al. (2000) and the observation nudging approach ("obs-nudging") of Stauffer and Seaman (1994) are applied.

*Analysis-Nudging FDDA Strategy:* In analysis nudging, the assimilation uses 3-D gridded analyses based on synoptic observations (Sec. 2.4), which are interpolated to the model's current time step. The modifications introduced by Shafran et al. (2000) to the FDDA prevent the application of the analyses below an arbitrary level (1.5 km AGL in this case) to avoid weakening mesoscale features generated in response to lower-boundary forcing. Thus, mesoscale features such as low-level jets and channeling around orography, that are not defined well by the synoptic upper-air observing network, but can be simulated by the MM5, are not inadvertently smoothed out of the model solutions.

Clearly, retention of the analysis nudging above 1.5 km directly influences the model solutions in the mid and upper layers of the atmosphere. However, it is important to note that by applying the analysis nudging to about 85 % of the atmosphere's mass, the normal hydrostatic and gravity-wave adjustments naturally lead to similar adjustments below 1.5 km. Thus, the modified analysis-nudging strategy remains very effective for reducing large-scale errors, such as phase speed errors in the deep synoptic-scale flow, through the entire model column. At the same time, it reduces the potential for detrimental interference with the model's physical and orographic solutions close to the surface.

*Observation-Nudging FDDA Strategy:* The special meteorological observations gathered during the SCOS-97 field study are appropriate for assimilation into the MM5 through observation FDDA (also referred to as obs-nudging). These data are used effectively on the 15-km and 5-km domains. The data tend to be clustered in the sub-region covered by the 5-km domain**,** with most of the observing sites located in and near the Los Angeles Basin. Outside that sub-region, the density of the special data decreases markedly. During intensive observing periods (IOPs), such as 21-24 September 1997, the data are temporally rich and allow better-than-normal definition of the evolving mesoscale circulations in the SoCAB and border areas that would be impossible to detect with only standard NWS synoptic data. Remote-sensing systems (radar wind profilers, RASS, SODARs) provided data hourly. Special radiosonde sites were operated four times a day. In addition, a network of about 180 surface stations provided meteorological data for the SCOS-97 data archive.

The observation-nudging strategy is based on PSU's FDDA work in complex terrain, described in Stauffer and Seaman (1994). The special SCOS-97 data (wind, temperature, moisture) from radiosondes, radar wind profilers, RASS, SODARS, and surface data were assimilated, after passing Level 2 quality assurance (Section 3.1). Only a few minor modifications were needed to the obs-nudging software for this case because Penn State has already built the necessary data interfaces to make use of SCOS-97 data as part of the ARB project supported under Contract No. 97-310.

### 2.2.2 FDDA for Surface Thermodynamic Variables

As part of a previous model-improvement study sponsored by ARB under contract No. 96-319, scientists at MCNC (led by Dr. Kiran Alapaty) and PSU (led by Prof. Nelson Seaman) collaborated on the development of a technique to assimilate surface temperature and humidity observations via FDDA to reduce errors in those important variable fields. Previous FDDA strategies in the MM5 neglected assimilation of surface-layer temperature because large errors could be introduced into the predictions for the boundary-layer depth (Stauffer et al. 1991). The problem with the original approach for assimilating surface thermodynamic data was that there was no adequate way to coordinate the effect of corrections made to the air temperature with their impact on the ground temperature. Thus, the surface sensible and latent heat fluxes could be disrupted by the FDDA, even changing sign in mid-day, which led to spurious oscillations in the surface fluxes, the surface air temperature, turbulence states and boundary-layer depth.

The new FDDA technique developed by Dr. Alapaty and Prof. Seaman uses these surface data to simultaneously nudge both the ground temperature and the temperature and mixing ratio in the atmospheric surface layer. The FDDA forcing for the ground temperature is calculated as modified surface fluxes for the sensible and latent heating, based on the errors in the model's predictions for the surface air temperature and humidity. This new approach has been described by Alapaty et al. (2001), which showed substantial reductions of errors in these variables. Since boundary-layer depth depends so much on the surface thermodynamics, this improvement in the FDDA strategy also reduces errors in that depth, which in turn can exert a great influence on air-chemistry concentrations. The new technique has already been introduced by PSU into the 3-D MM5, so that surface temperature analyses (with or without special local observations) can be assimilated routinely into the model. Recently, the technique was used by PSU to generate meteorological fields for a regional air-quality study of visibility and aerosols over the Big Bend National Park (BRAVO).

Although the new FDDA strategy of Alapaty et al. (2001) has not yet been released through NCAR, it has considerable potential for reducing errors in the thermodynamic and boundary-layer depth fields over the SoCAB and border regions with Mexico that are the foci of the proposed study. Thus, after ARB approval, it was included as a supplemental experiment in the present study (Section 3.2). By applying the new approach in a separate experiment, its influence can be isolated and more easily evaluated.

## 2.3 Domain Structure

*Horizontal Structure:* For all applications of MM5 on the expanded SoCAB domain the model configuration was as follows. Four nested grids of 135-, 45-, 15- and 5-km were used (see **Figure 4**). These domains cover regions that are mostly similar to those described in Bornstein et al. (2001), but with the 5-km domain extended southward and eastward as requested by ARB (see **Figure 5**). The large area covered by the outermost domain (135-km mesh size) is important to reduce the impact of uncertainties in the upwind meteorological boundary

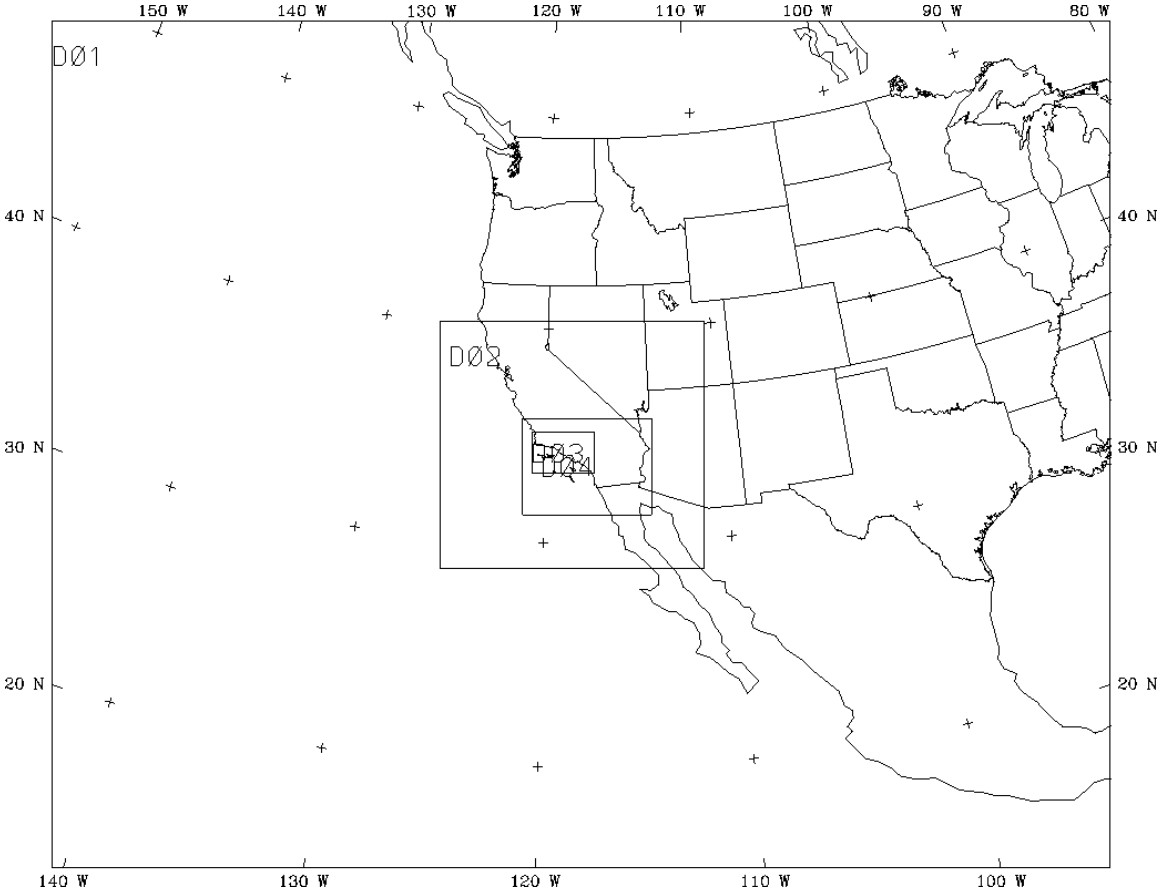


**Figure 4.** Configuration of the MM5 nested-grid domains. Domain 1 resolution is 45 km. Domain 2 resolution is 15 km. Domain 3 resolution is 5 km. Domain 4 resolution is 1.667 km. (The 1.667-km domain has not been used in any runs produced during this study.)

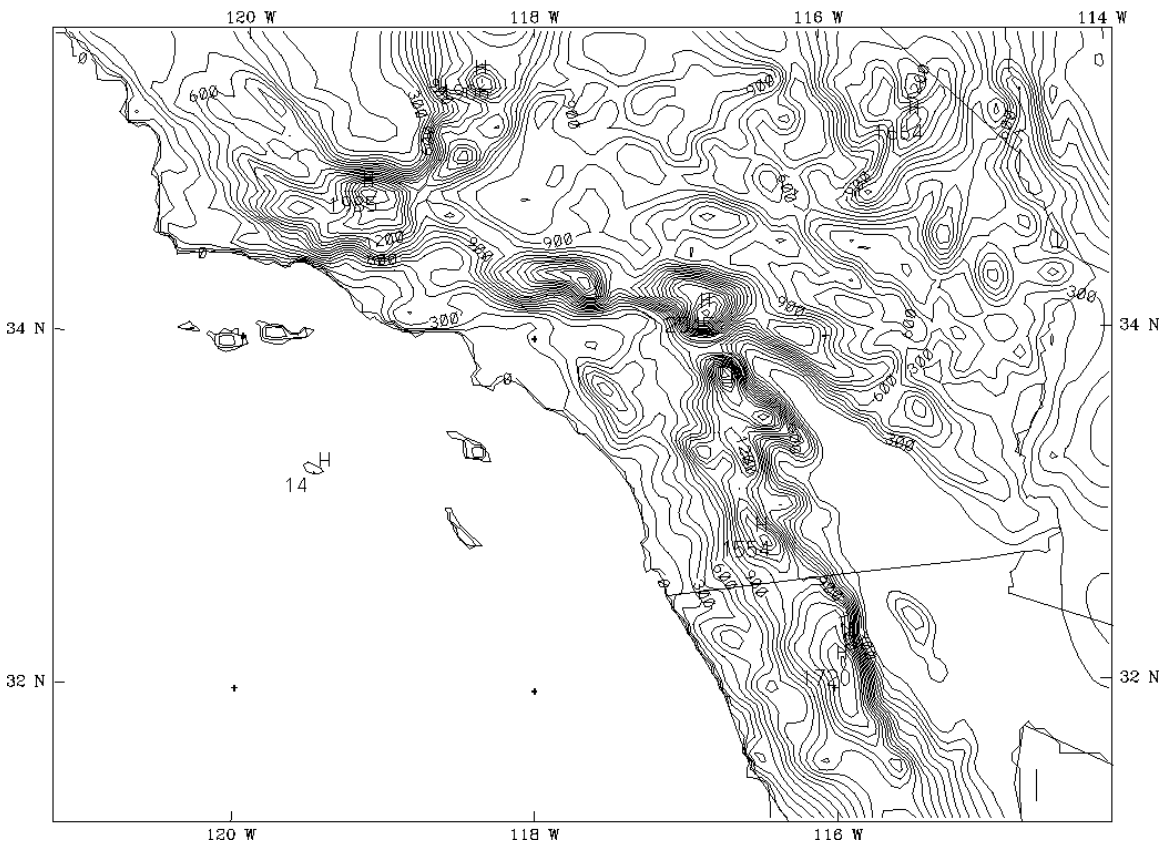


**Figure 5.** Terrain (m) on the extended 5-km domain of the MM5 nested mesoscale model for the current project supported by ARB under Contract No. RFP 00-719. Contour interval is 100 m. Size of the 5-km domain is 133 X 100 points (132 X 99 grid cells).

conditions over the data-sparse Pacific Ocean. The coarse grid (135 km) has its center at 34.5370 N, 118.0 W, which defines the orientation of all four domains. The domains shown in the figures use the Lambert conformal secant projection, with reference latitudes at 30.0 N and 60.0 N.

In its RFP, ARB requested that the southwest corner of the 5-km domain should lie at 150 km Northing and -300 km Easting. This corresponds to $60\,\Delta X$ west of the coarse-grid center and $70\,\Delta Y$ south of the same center (where $\Delta X = \Delta Y = 5$ km). The RFP also specified a 5-km domain of 130 X 98 grid cells (131 X 99 points). Unfortunately, that number of points created an incompatibility with one of the constraints for defining the MM5 nested grids. That is, the number of grid cells in a nested domain must be a multiple of three in order to correctly specify the grid-interface conditions from its parent (next coarser) domain.

However, we understand that ARB's intent was to ensure exact compatibility between the 5-km MM5 domain and the domain of its photochemical model (with its pre-mapped gridded emissions). Thus, Penn State proposed a slight further expansion of the 5-km domain that we believe meets ARB's goals and also maintains the nested-grid compatibility requirements of the MM5. For the 5-km domain shown in **Figure 5** the southern boundary has been extended farther southward by 1 $\Delta Y$ and the eastern boundary is extended farther eastward by 2 $\Delta X$, relative to ARB's proposed domain. The coarse-grid center was unchanged by this adaptation, thus maintaining the desired grid alignment. The result is a 5-km domain having 132 X 99 grid cells (133 X 100 points), with its southwest corner at 145 km Northing and -300 Easting. The northern and western boundaries of the 5-km domain remain identical to those in the prior SCOS-97 cases run under Contract 97-310, as in ARB's design for this project. This slight reconfiguration was presented to ARB at the beginning of the project and accepted as meeting all of ARB's goals, while allowing for the constraints imposed by the MM5's 3:1 mesh ratio.

*Vertical Structure:* Originally, Penn State configured the MM5 with 40 layers in the vertical direction from the surface to the model top at 50 mb. The high model top (~20 km MSL) was chosen to accommodate a deep stratospheric layer in the upper atmosphere of the model domain. By having the model extend farther into the stratosphere, a deep stabilizing layer was provided to safely decelerate any violent thunderstorm updrafts that might occur in regions having deep convection. Convection was at least a possibility in the 21-24 September 1997 case. (This episode included a strong tropical cyclone moving northward from southern Baja California to the mouth of the Colorado River over a period of 3-4 days. Based on satellite images, areas of strong deep convective and heavy rainfall were expected in the outer three domains, with some convection possible inside the 5-km domain, as well.)

At the project kick-off, ARB scientists requested that additional resolution be provided in the region of about 2-3 km AGL (above ground level). It was pointed out, quite correctly, that the planetary boundary layer in desert regions of southern CA and northern Mexico often approach 3 km. The originally proposed vertical distribution of layers (not shown) would have given rather coarse resolution in the upper part of those very deep PBLs. In response Penn State added five layers concentrated in the region between 2 and 3 km AGL, and produced a new set of model layer definitions that was used in all model experiments discussed in this report (**Table 1**).

**Table 1.** Meteorological-model vertical sigma levels and corresponding layer heights[1] (m) compatible with photochemical-model sigmas defined by ARB (see **Table 2**). Heights are based on a model top at 50 mb. Layer numbers are listed upward from the ground. (Note: Internally, the vertical index in MM5 increases downward from the top of the model toward the surface.)

| Layer No. | Sigma | Height (m) | Layer No. | Sigma | Height (m) |
|---|---|---|---|---|---|
| Surface | 1.000 | 0 | 23 | 0.800 | 1782.7 |
| 1 | 0.997 | 25.0 | 24 | 0.785 | 1927.9 |
| 2 | 0.992 | 66.9 | 25 | 0.769 | 2085.1 |
| 3 | 0.986 | 117.2 | 26 | 0.752 | 2254.9 |
| 4 | 0.980 | 167.8 | 27 | 0.734 | 2437.8 |
| 5 | 0.973 | 227.0 | 28 | 0.714 | 2645.0 |
| 6 | 0.966 | 286.4 | 29 | 0.692 | 2878.0 |
| 7 | 0.958 | 354.7 | 30 | 0.668 | 3138.7 |
| 8 | 0.950 | 423.3 | 31 | 0.640 | 3451.9 |
| 9 | 0.942 | 492.3 | 32 | 0.601 | 3906.0 |
| 10 | 0.934 | 561.6 | 33 | 0.552 | 4510.7 |
| 11 | 0.926 | 631.3 | 34 | 0.508 | 5087.9 |
| 12 | 0.918 | 701.3 | 35 | 0.464 | 5706.0 |
| 13 | 0.910 | 771.8 | 36 | 0.414 | 6457.5 |
| 14 | 0.902 | 842.6 | 37 | 0.368 | 7196.6 |
| 15 | 0.892 | 931.6 | 38 | 0.322 | 7992.3 |
| 16 | 0.882 | 1021.3 | 39 | 0.276 | 8859.5 |
| 17 | 0.874 | 1093.5 | 40 | 0.230 | 9823.5 |
| 18 | 0.866 | 1166.1 | 41 | 0.184 | 10927.8 |
| 19 | 0.853 | 1284.9 | 42 | 0.138 | 12249.6 |
| 20 | 0.840 | 1404.9 | 43 | 0.092 | 13889.6 |
| 21 | 0.827 | 1526.2 | 44 | 0.046 | 16135.0 |
| 22 | 0.814 | 1648.9 | 45 | 0.000 | 19865.1 |

[1]Note: By design, the sigma levels in **Table 1** that correspond to layer boundaries of the photochemical model also appear in **Table 2**. This ensures that the meteorological-model layers can be consolidated easily into the photochemical-model layers without vertical interpolations. However, the heights of these corresponding levels in **Tables 1 and 2** do not match. There are two reasons for the mismatches in the heights. First, the resultant heights depend on the assumed temperature profile used in the hypsometric equation used when making the calculations. (It appears that the temperature profile used in ARB's height calculations was rather cold compared to the standard atmosphere). Second, the layer heights are also dependent on the pressure defined for the model top. In **Table 1**, we have assumed a model top at 50 mb, as discussed above in this section. It is likely that ARB assumed a model top at 100 mb in its calculations. These differences are not difficult to reconcile.

The MM5's vertical structure was configured so that the top and bottom of each chemistry-model layer will coincide with the boundaries of meteorological-model layers (compare **Tables 1 and 2**). The number of meteorological model layers in each chemistry model layer will be an integer (one or two), so that the meteorological solutions can be easily consolidated onto the chemistry-model grid. This approach will ensure that no vertical interpolations are needed when preparing the meteorological inputs for the photochemical model. Moreover, the use of 45 layers represents an increase of 15 layers from the MM5 configuration used by Bornstein et al. (2001). Most of the additional layers have been placed in the lower atmosphere, so that there are 24 layers below 2 km above ground level (AGL) (compared to 12 layers below this level in the earlier study). The additional vertical resolution in the MM5 is intended to improve the model's ability to resolve thin re-circulation flows that are common in the Los Angeles Basin and perhaps occur in other areas of the SoCAB. Also, the first calculation level in this layer distribution (midway through the first layer) is at approximately 12 m AGL, which is about the height of most surface wind observations. Consequently, surface-wind verification should be quite direct.

**Table 2.** Photochemical-model vertical sigma levels and corresponding layer heights (m) supplied by ARB. Sigma levels are relative to the meteorological model (**see Table 1**).

| **Layer Number** | **Sigma** | **Height (m)** |
|---|---|---|
| Surface | 1.000 | 0.0 |
| 1 | 0.992 | 58.1 |
| 2 | 0.980 | 146.0 |
| 3 | 0.966 | 249.6 |
| 4 | 0.950 | 369.3 |
| 5 | 0.934 | 490.4 |
| 6 | 0.918 | 613.1 |
| 7 | 0.902 | 737.4 |
| 8 | 0.882 | 879.1 |
| 9 | 0.866 | 1022.9 |
| 10 | 0.840 | 1234.5 |
| 11 | 0.814 | 1450.8 |
| 12 | 0.777 | 1767.4 |
| 13 | 0.740 | 2094.8 |
| 14 | 0.650 | 2480.8 |
| 15 | 0.552 | 3448.4 |
| 16 | 0.464 | 4986.1 |

## 2.4 Initialization and Lateral Boundary Conditions

Initial conditions (ICs) and lateral boundary conditions (BCs) for the MM5 are specified from 45-km objective analyses performed on pressure levels at 12-h intervals (Benjamin and Seaman 1985). Over the data-sparse oceans the analyses are essentially those supplied through the first guess (background) fields obtained from archives of the global spectral analyses performed by the National Centers for Environmental Prediction (NCEP) for the global Global Forecast System (GFS). Surface and upper-air observations from the National Weather Service (NWS) were collected from Penn State and NCAR data archives for use in the objective analyses. All observations were quality-checked by the MM5 pre-processors using automated gross-error checks and "buddy" checks. In addition, the radiosondes undergo a vertical consistency check. None of the special SCOS data are used in the objective analyses because they are almost entirely restricted to the SoCAB, where their density is unrepresentative of most land areas. The special data are assimilated through obs-nudging (Sec. 2.2).

Following the objective analysis on pressure levels and at the surface, the fields are interpolated in the vertical to the model's sigma levels to complete the ICs for the 45-km analysis domain. For the model's other two finer-resolution domains (see Sec. 2.3), the initial fields are obtained by interpolation from the 45-km analyses. The sea-surface temperature analyses are obtained from NCEP and from the U.S. Navy and the values of these fields are held constant for the duration of each experiment. In addition, based on satellite imagery and climatology, snow is assumed to be unimportant in the SoCAB during the SCOS-97 episode.

Another initial field that must be defined for the MM5 is the deep-soil temperature below the surface, $T_m$. It is nominally defined at ~25 cm depth, where the soil temperature is assumed to be approximately invariant between day and night. The default value of $T_m$ is calculated in the data preprocessors by averaging all of the 12-h surface-layer temperature analyses (at 0000 UTC and 1200 UTC) for the entire episode. This averaged $T_m$ field is held constant through the model simulation. The default value of $T_m$ is sometimes inconsistent with true conditions due to changing meteorological states. Therefore it is sometimes necessary to modify the default $T_m$ value based on evaluations of base model experiments and data analysis.

A special characteristic of the PSU analysis scheme designed for applications in CA, not available in the standard NCAR pre-processors, is that the low-level coastal temperature and moisture observations are not used uniformly in the onshore and offshore directions. They are only used in the upwind direction because they are generally not representative of both regimes simultaneously. The analysis scheme first analyzes the wind direction at stations within the coastal zone and determines whether onshore or offshore flow exists. The temperature and moisture data are then applied only in that portion of the standard area of influence around those coastal sites that lies upwind (i.e., either over land or ocean, depending on wind direction). This approach is applied only in the lowest kilometer and can be important for preserving the low-level coastal gradients that characterize the near-shore zone of California.

Lateral boundary information is introduced into the model using the Davies and Turner (1977) relaxation technique. The relaxation is applied in the outermost five rows and columns of the

outer (synoptic scale) domain (Sec. 2.3), with boundary values defined by interpolating between successive 12-h analyses of the same type used to define the ICs. This approach gradually and continuously imposes the observed state at the boundaries without generating large imbalances between the observed and modeled states. One-way interface conditions are used in this study between the 45-km domain and the 15-km domain, and also between the 15-km and 5-km domains, so the values of the prognostic variables at the interior interfaces are supplied from the next coarser grid. No feedback of information is allowed from the finer grids to the coarser grids in these domains.

# 3. DATA PREPARATION AND EXPERIMENT DESIGN

## 3.1 Special SCOS-97 Data Preparation and Quality Assurance

The 1997 SCOS field study produced a meteorological data archive that includes hourly measurements from 27 Radar Wind Profilers (RWP) and ~180 surface sites. Data validation is critical because erroneous individual data values can cause serious errors in modeling results. The problem is two-fold. First, the data are assimilated into the MM5 through obs-nudging FDDA to minimize error growth (Sec. 2.2.1 and 3.2). If the assimilated data are in error, the model solution will be pushed in the wrong direction over a wide region. (Note that only two of the experiments use the obs-nudging option. The other experiments withhold the special SCOS-97 observations as an independent dataset used only for model verification.) Second, the observations are used for evaluating all of the model simulations. Erroneous information in the validation dataset will raise the statistical error scores used to evaluate model accuracy.

Data validation consists of quality control (QC) procedures developed to identify deviations from measurement assumptions and procedures. A level of validation is a numeric code indicating the degree of confidence in the data. These levels provide some commonality among data collected at various places and quality controlled by different agencies to help ensure that all data have received a comparable level of validation. Various data validation levels applied to air quality and meteorological data have been defined by Mueller and Watson (1982) and Watson et al. (1989). Four levels of data validation are summarized in **Table 3**.

STI performed the Level 1 validations on the SCOS-97 RWP data during the SCOS-97 field study under contract to ARB and served as the primary data repository. The RWP data were subjected to Level 2 validation at STI. The goal of Level 2 validation is to evaluate spatial and temporal consistency in the data. Here, STI performed the Level 2 validation by comparing observations to external data sources. The external sources used in this study are summarized in **Table 4**. Note that "external" does not necessarily mean independent. Much of the analysis performed in Level 2 validation involves comparing observations at individual sites with those from other sites in the same dataset. Level 2 validation also affords an opportunity to re-evaluate data that were flagged as "suspect" in the Level 1 validation. While some of the comparisons performed during Level 2 validation are quantitative, there is a greater reliance on qualitative reviews. Staff meteorologists who understand the measurement systems and the meteorological processes expected to be contained in the data have performed the qualitative reviews.

**Table 3.** Data validation levels.

| Level | Description |
|---|---|
| 0 | Level 0 data validation is essentially raw data obtained directly from the data acquisition systems in the field. Level 0 data have been reduced and possibly reformatted, but are unedited and unreviewed. These data have not received any adjustments for known biases or problems that may have been identified during preventive maintenance checks or audits. Routine checks are made during the initial data processing and generation of data, including proper data file identification, review of unusual events, review of field data sheets and result reports, instrument performance checks, and deterministic relationships. |
| 1 | Level 1 data validation involves quantitative and qualitative reviews for accuracy, completeness, and internal consistency. Quantitative checks are performed by software screening programs, and qualitative checks are performed by meteorologists or trained personnel who manually review the data for outliers and problems. QC flags, consisting of numbers or letters, are assigned to each datum to indicate its quality. Data are only considered at Level 1 after final audit reports have been issued and any adjustments, changes, or modifications to the data have been made. |
| 2 | Level 2 data validation involves comparisons with other independent data sets. This includes, for example, inter-comparing collocated measurements or making comparisons with other measurement systems or analyses. This level is often part of the data interpretation or analysis process. |
| 3 | Level 3 validation involves a more detailed analysis when inconsistencies in analysis and modeling results are found to be caused by measurement errors. |

**Table 4**. External data sources used during Level 2 data validation.

| External Data Sources | Explanation of Usage |
|---|---|
| NWS upper-air soundings | Perform reasonableness checks on the upper-level profiler wind and temperature data. |
| NWS upper-air meteorological charts | Perform reasonableness checks to evaluate the spatial consistency of the upper-level winds based on geopotential height gradients depicted on 700 mb and 850 mb charts. |
| NWS surface meteorological charts | Track synoptic scale weather features (i.e., frontal positions, thunderstorms) that may affect instrument performance or data quality. |
| Satellite images | Track synoptic-scale weather features (i.e., frontal positions, thunderstorms) that may affect instrument performance or data quality. |
| Profiler/RASS data from other sites | Perform checks of temporal and spatial consistency. |
| Surface data from other sites | Check for temporal and spatial consistency in the wind speed, wind direction, and temperature data. |
| Maps of terrain and land use | Check for consistency of winds and temperature with terrain and land use characteristics. |

As part of the Level 2 validation process, the RWP data were displayed, analyzed, and edited using GraphXM, a STI software product developed specifically for these purposes. GraphXM is used to generate standard time-height cross sections of the RWP data, which then are inter-compared with the cross sections from other profiler sites and analyses from other external data sources. An example of this type of analysis is shown in **Figure 6**.

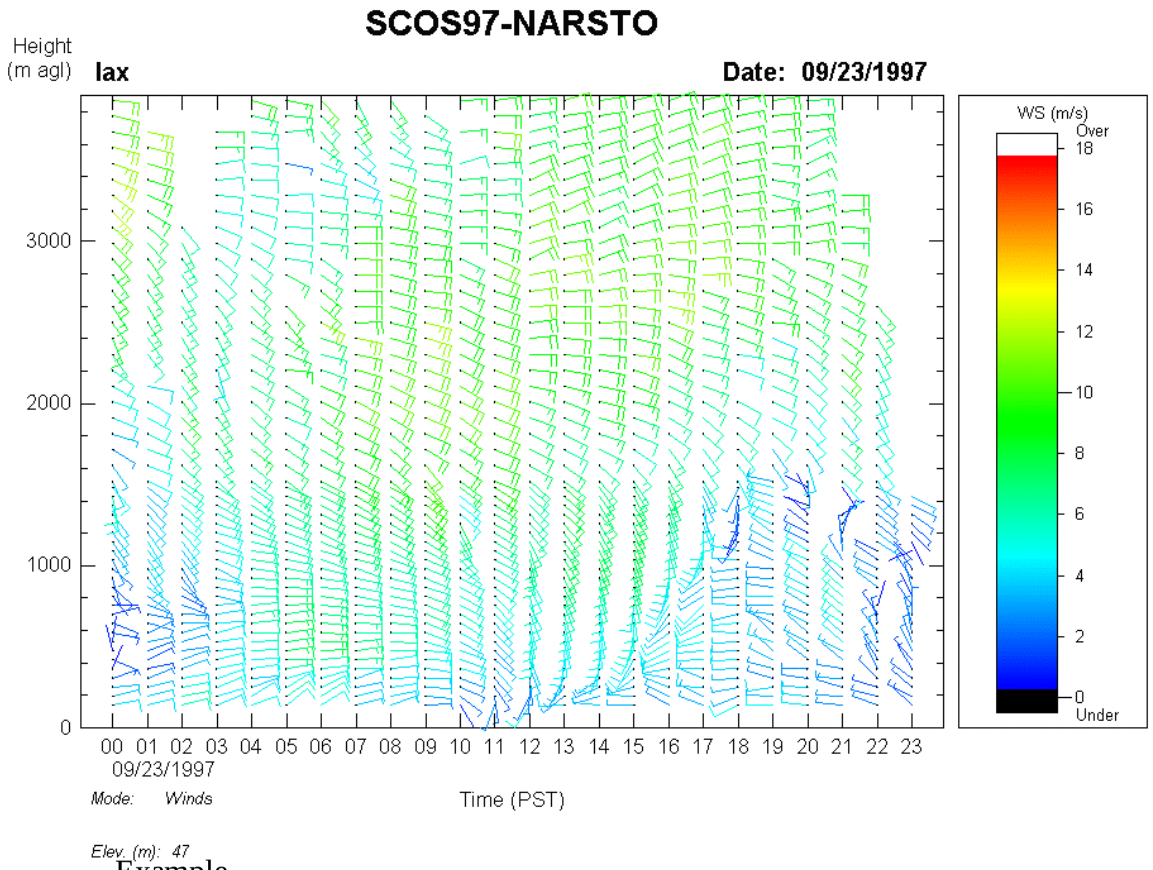


**Figure 6.** Example time-height cross section of the RWP data plotted by GraphXM, 23 September 1997.

As the data underwent Level 2 validation, all changes to the original quality control codes or data were documented in log files that will be provided with the final Level 2 datasets. The same quality control codes that have been used throughout the SCOS-97 program (see **Table 5**) have been used in this study to flag missing, inconsistent, or suspect data. The final Level 2 quality-controlled data have been combined into flat ASCII files, in consultation with the ARB contract manager.

**Table 5.** Quality control codes.

| QC Code | QC Code Name | Definition |
|---|---|---|
| 0 | Valid | Observations that were judged accurate within the performance limits of the instrument. |
| 1 | Estimated | Observations that required additional processing because the original values were suspect, invalid, or missing. Estimated data may be computed from patterns or trends in the data (e.g., via interpolation), or they may be based on the meteorological judgment of the reviewer. |
| 2 | Calibration applied | Observations that were corrected using a known, measured quantity (e.g., instrument offsets measured during audits). |
| 3 | Unassigned | Reserved for future use. |
| 4 | Unassigned | Reserved for future use. |
| 5 | Unassigned | Reserved for future use. |
| 6 | Failed automatic QC check | Observations flagged with this QC code did not pass screening criteria set in automatic QC software. |
| 7 | Suspect | Observations that, in the judgment of the reviewer, were in error because their values violated reasonable physical criteria or did not exhibit reasonable consistency, but the specific cause of the problem was not identified. |
| 8 | Invalid | Observations that were judged inaccurate or in error, and the cause of the inaccuracy or error was known. |
| 9 | Missing | Observations that were not collected. |

STI obtained what was described as Level 1 surface meteorological data from the ARB. However, in processing the surface meteorological data for this episode, it was apparent that not all of the data had undergone Level 1 validation. Therefore, STI performed additional data validation including automated range checks, time-series analysis, and spatial analysis of the data before preparing the final surface meteorological datasets for use in FDDA and model performance evaluation. Figure 7 provides and example of the types of graphical analyses used in the data validation.

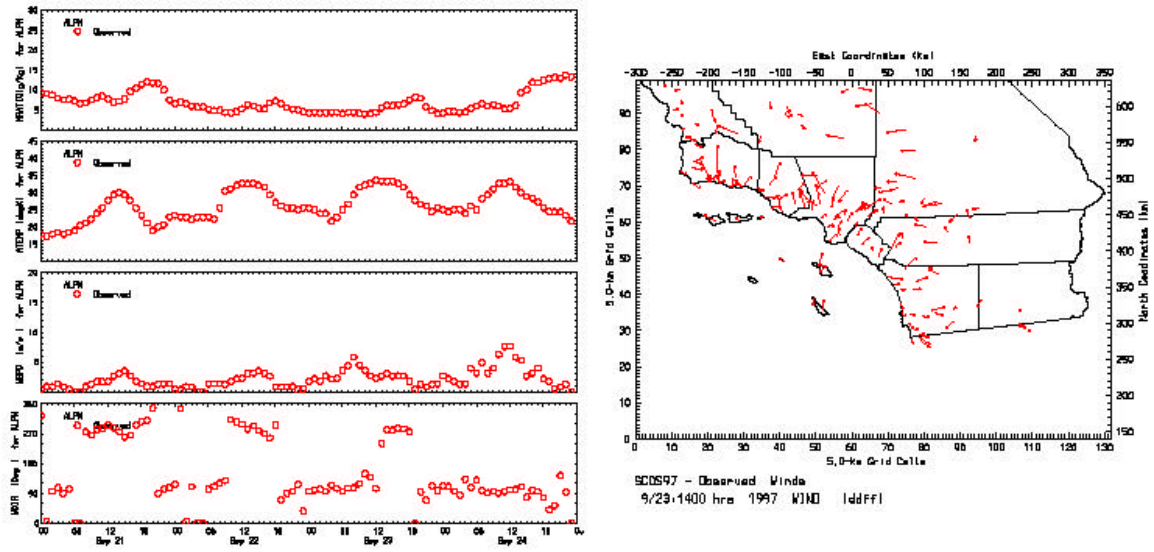

**Figure 7**. Example of analyses prepared to validate the surface meteorological data.

### 3.2 Experiment Design

*Distribution of layers:* All of the experiments performed for this study used the first three domains shown in Figure 4 and the 45 vertical layers were distributed as reported in Table 1 (Section 2.3). The model top was placed at 50 mb. As shown in this table the thickness of the lowermost model layer is 25 m. Because the grid design of the MM5 model (Grell et al. 1994) has a staggered mesh system in the vertical (and horizontal) direction, the computation level for most prognostic variables ($u$, $v$, $T$, $q$, $p'$) is at the middle of each layer. This places the height of the lowest computation level at 12.5 m AGL, or about the height of a standard 10-m wind measurement tower. Above the surface layer, the grid gradually "telescopes" outward to create thicker layers farther aloft. Thus, for the LA Basin where PBL depth may typically be on the order of 300-600 m, the domain configuration yields about 6-10 layers in the shallow PBL. On the other hand in the desert regions of southeastern CA and northern Mexico where PBL depths often reach 2-3 km, the model will represent the PBL with about 25-30 layers. Even with the PBL top at 3 km, the upper part of the PBL will be represented with model layers having thickness no more than 260 m. The thickest layers in the first 1000 m AGL are only 90 m deep. This provides excellent vertical resolution for the study of boundary layer transport and recirculation.

*Length of Simulations and Spin-Up Period:* Following consultation with ARB at the project kick-off meeting held in Sacramento, 5 February 2002, the period of simulation for the MM5 experiments was defined as the four days (96 h) from 0000 GMT, 21 September 1997 (1700 PDT, 19 September) through 0000 GMT, 25 September (1700 PDT, 24 September). This period begins 12 h earlier than the period of interest defined by ARB to allow for spin-up of the numerical atmospheric chemistry in subsequent model experimentation. Only about 6-8 h of

dynamical spin-up time is required for the MM5 to come into dynamic balance from the initial state. It is expected that the comparatively brief 12-h chemistry spin-up is sufficient because the generally clean air entering the SoCAB and Baja California from the Pacific Ocean means that local emissions within the region should dominate the chemistry, rather than inter-regional advection. Also, the time period with highest concentrations of pollutants occurs in the latter half of the episode, on 22-23 September.

*Land use Adaptations for CA and Mexico*: Penn State's experience with modeling domains over CA has consistently shown that some of the default land-use categories in the MM5's look-up tables (Sec. 2.1) are not well-suited to conditions in CA. The dry climate of the region, coupled with extensive irrigation of agricultural areas, can lead to significant errors in surface heat and moisture fluxes when the default values are used. Therefore, the moisture availability of all land-use categories (other than water bodies) is set to one-half the default values for the SCOS-97 domains. This is the routine approach found valid in many CA modeling studies conducted by PSU and is consistent with the late summer season in regions having a Mediterranean climate, where there typically will be virtually no rainfall from Spring to the middle of Autumn.

*Description of Experiments*: Four primary numerical experiments were proposed by Penn State: A control without FDDA, an experiment with conventional analysis-nudging FDDA, an experiment with multi-scale FDDA (analysis nudging and obs-nudging), and a final experiment with that repeats the third, but adds the surface FDDA technique described by Alapaty et al. (2001). The third experiment, multi-scale FDDA, is the ***base-case simulation*** referred to in ARB's RFP 00-719.

After discussions with ARB during a kick-off meeting at the beginning of the project, Penn State agreed to delete the original 135-km outer domain that was proposed and to extend the next-finer mesh (45-km) to cover the area of the 135-km domain. This is clearly a better option because it keeps the lateral boundaries very far from the region of interest, while improving the grid resolution with which the synoptic-scale meteorology is represented. Penn State also agreed to consider an optional 1.667-km inner domain over the LA Basin and Santa Barbara Channel. This very-high resolution domain would be run for one experiment (most likely the base-case simulation), only if model evaluations indicated that the 5-km domain was not resolving the flow in the September 21-24, 1997, episode.

Early experimentation with analysis nudging showed that the wind fields were quite realistic and that the temperature field was biased toward cold temperatures. Investigation of the results indicated that the NCEP sea -surface temperatures were too cold in the region offshore from the SoCAB. Also, it was found that the deep-soil temperature in the first model experiment (which is set at a constant and is dependent on the season) was too cold by 4-6 C in this case. As a result, Penn State recommended that a second analysis nudging experiment be performed. The objective of the 2$^{nd}$ analysis nudging experiment was to raise the MM5's constant deep-soil temperature by 6 C and to install a new 9-km NASA SST data set. The results from the extra experiment were rather successful (details described in Section 5). Therefore, this report will discuss a total of five experiments:

1. *Control Experiment*: The control experiment (Exp. 1) uses no data assimilation on any of the three active domains (45 km, 15 km and 5 km). Lateral boundary conditions on the 45-km domain are forced from NCEP global analyses. The interface conditions for the nested domains are forced by the next outer domain using one-way nesting techniques (no feedback to the parent mesh). The deep soil temperature (land) was set to 4 C colder than the default MM5 value (the default is calculated as the average of the 1200 GMT and 0000 GMT surface temperature reported in the analyses of the simulation period). The sea-surface temperatures (SSTs) were interpolated from the global one-degree horizontal resolution (~111 km) ocean temperatures archived by NCEP.

2. *Conventional Analysis-Nudging FDDA*: This experiment (Exp. 2) uses standard analysis nudging on the two outer domains having mesh sizes of 45 km and 15 km. No analysis nudging is used on the 5-km domain. Lateral boundary conditions interface conditions are identical to those in Exp. 1. The assimilation is based on the well-tested strategy reported by Shafran et al. (2000) described in Section 2.2.1. The deep soil temperature (land) is also the same as in the Control experiment (4 C colder than the default MM5 value) and SSTs are those based on the NCEP analyses.

*2.5* *Conventional Analysis-Nudging FDDA with Modified Soil and Sea Temperatures*: This supplemental experiment (Exp. 2.5) repeats the analysis nudging strategy used in Exp. 2, but with modifications to the lower boundary-condition temperatures. First, the NCEP sea-surface temperatures are replaced by a higher-resolution 9-km data set from NASA, based on buoy-corrected satellite infrared measurements (**Figure 8**). To do this, data SSTs were obtained on the web at http://podaac.jpl.nasa.gov/sst/sst_data.html (provided by Physical Oceanography-Distributed Active Archive Center, Jet Propulsion Laboratory, California Institute of Technology in partnership with Raytheon Corp.). The NASA SSTs are interpolated to the MM5 5-km grid, resulting in temperatures in the

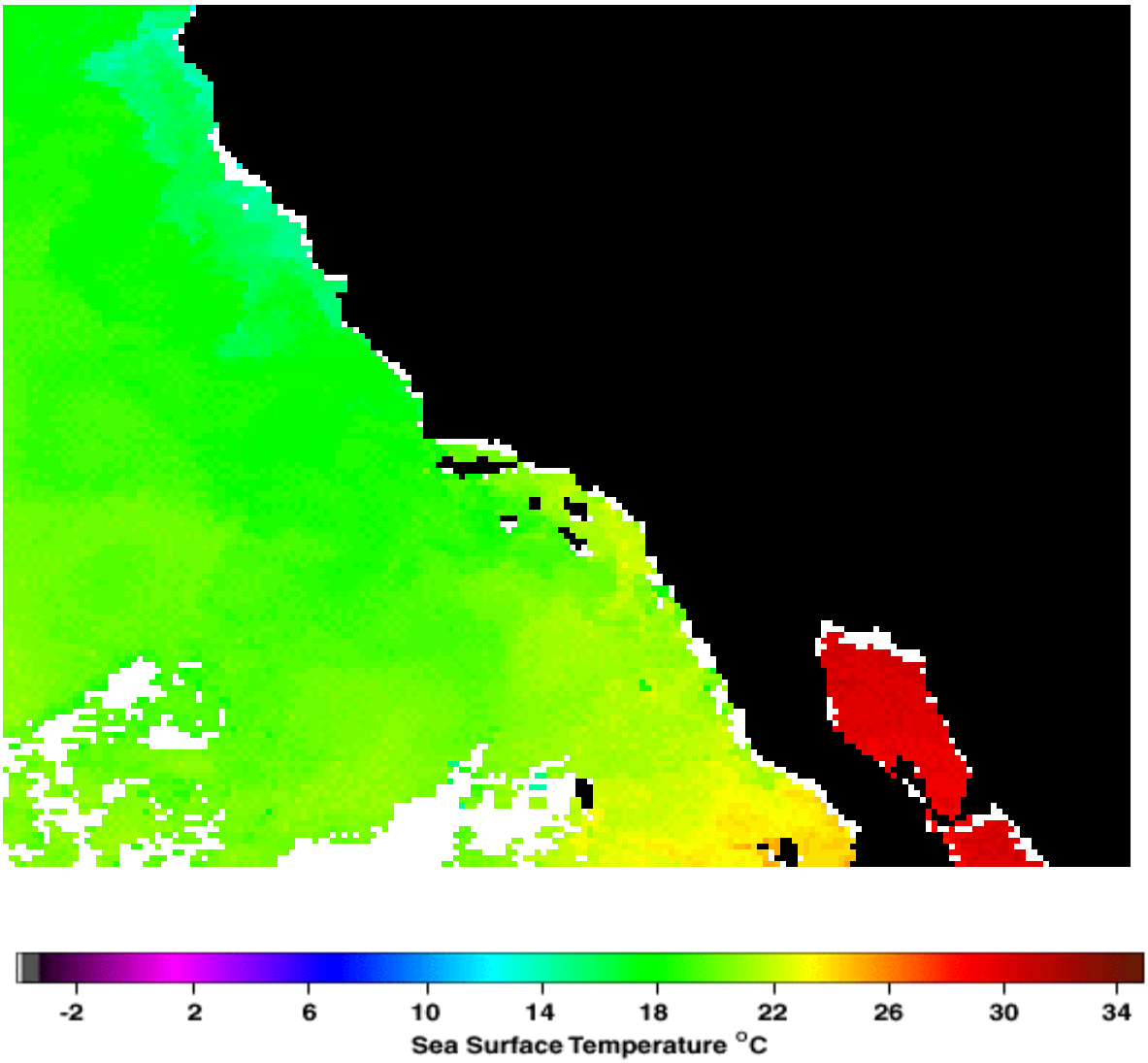


**Figure 8.** Observed nighttime sea-surface temperatures (C) over the CA Bight at 9-km resolution, from NASA AVHRR infrared imagery, 21 September 1997.

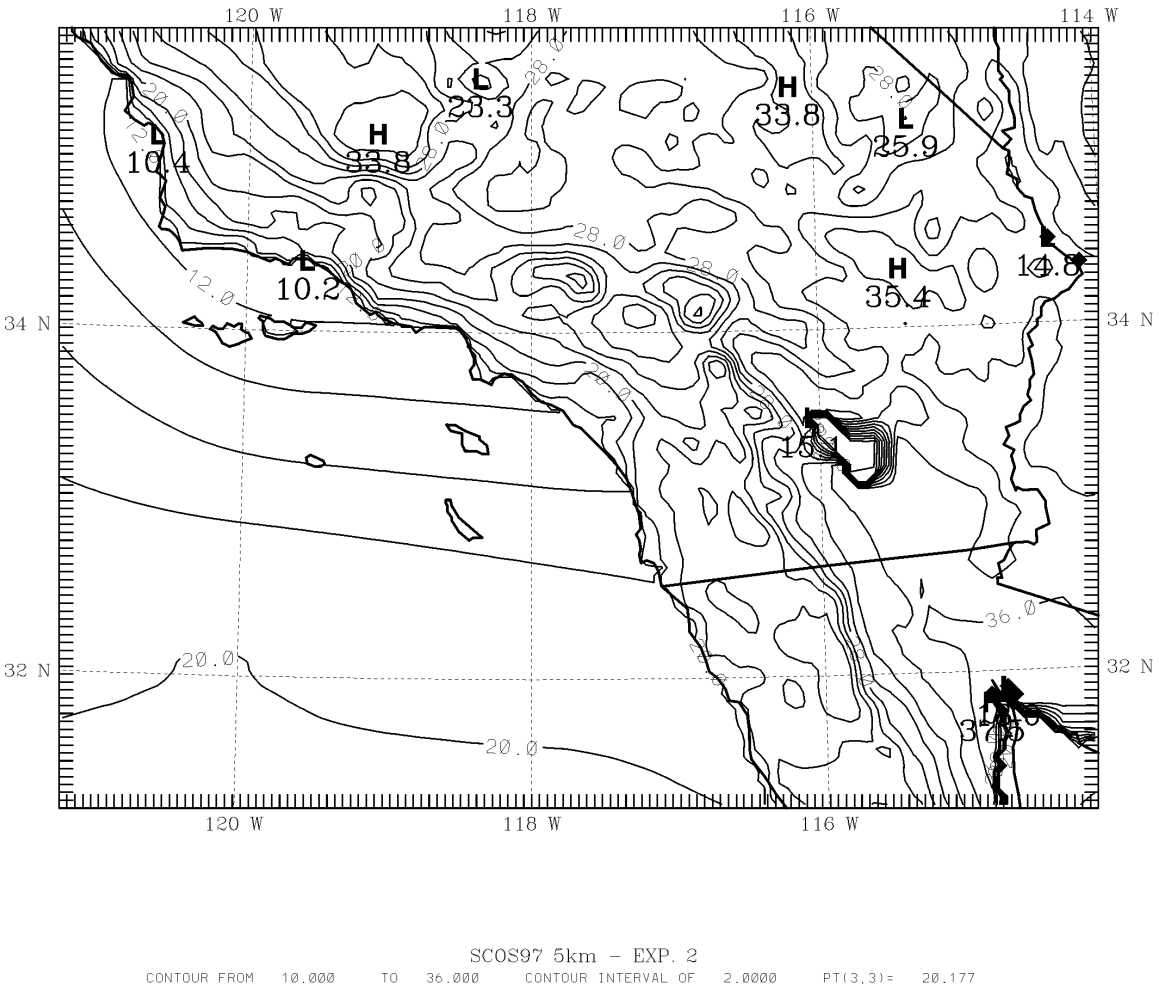


**Figure 9.** Ground temperature field (C) on the 5-km domain for 21 September 1997, 0000 UTC showing (a) original sea-surface temperatures interpolated from NCEP global analysis, (b) final sea-surface temperatures interpolated from NASA AVHRR infrared analysis. Contour interval is 2 C.

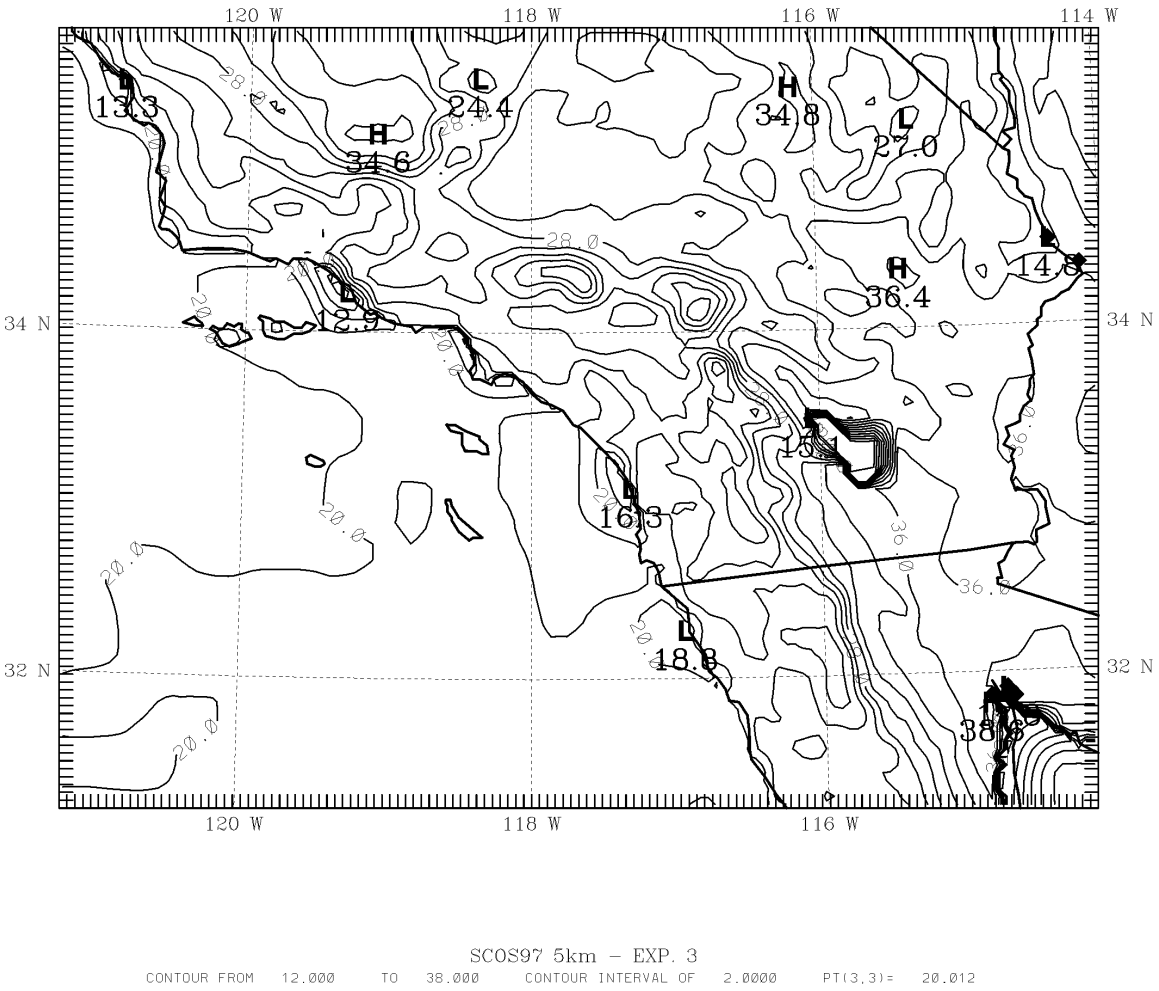


**Figure 9b (cont'd).**

CA Bight that are generally 4-8 C warmer than in the NCEP analyses (**Figure 9**). The warmer water should have two major effects on the meteorology over the SoCAB during this episode: the sea breeze should be weaker due to reduced land-sea thermal contrast, and temperatures over coastal regions should be warmer due to weaker cold advection. Second, the deep soil temperature definition over land is changed to be 2C warmer than the MM5 default setting (6C warmer than in Exps. 1 and 2). The latter change is justifiable for a late September episode in the SoCAB region because the length of darkness is rapidly growing while the deep soil is at or near its annual maximum. Thus, the mean the 0000 GMT and 1200 GMT temperatures is apt to be cooler at this time than the deep soil. Although there are no soil temperature measurements available to prove this hypothesis, it is implied by the results of Exp. 1 and is consistent with standard soil climatologies. (The MM5 does not have a significant known mean surface temperature bias, when averaged over warm and cold seasons, unless the soil temperature is specified incorrectly).

3. *Conventional Multi-Scale FDDA (analysis & observation nudging):* Experiment 3 is similar to Exper. 2.5 (analysis nudging plus modified soil/sea temperatures), but with the addition of *obs nudging* on the 15-km and 5-km domains. The assimilation of the observations is based on the well-tested strategy reported by Stauffer and Seaman (1994) described in Section 2.2.1. Experiment 3 is the **"base-case" simulation** referred to in ARB's RFP 00-719.

4. *Observation FDDA with new Surface FDDA:* Experiment 4 is similar to the Multi-Scale FDDA Exper. 3, but with the addition of surface FDDA on all domains (Alapaty et al. 2001). This experiment is listed last in the suite of runs because it adds a new and comparatively less-tested strategy for assimilating 3-h surface analyses of temperature and moisture (analysis nudging), as described in Section 2.2.2. The surface nudging function for the domains are as follows: On the 45-km domain, $G = 9 \times 10^{-4}\ s^{-1}$. On the 15-km domain, $G = 6 \times 10^{-4}\ s^{-1}$. Finally, on the 5-km domain, $G = 3 \times 10^{-4}\ s^{-1}$. The 5-km and 15-km surface analyses include the special SCOS-97 data sets to supply mesoscale detail to the model.

# 4. DESCRIPTION OF THE 21-24 SEPTEMBER 1997 EPISODE

## 4.1 Air Quality

From an air quality standpoint, the high ozone concentrations at sites near the United States-Mexico border were of greatest interest during this period. On 23 September, the ozone concentrations at sites near Mexicali and Calexico began to rise rapidly at 0800 PDT and reached peaks ranging from 117 to 223 ppb between 0900 and 1300 PDT. This event is depicted in **Figure 10**, which includes ozone time-series for 4 sites in Mexicali and 3 sites in Calexico: (1) Collegio de Bachilleres -Mexicali (MEXA), (2) Technical University-ITM-Mexicali (MEXI), (3) University of Baja California-Mexicali (MEXU), (4) CBTIS-Mexicali (MEXT). (5) Calexico Grant Street (CLXC), (6) Calexico East (CLXE), and (7) Calexico Ethel Street (CALE).

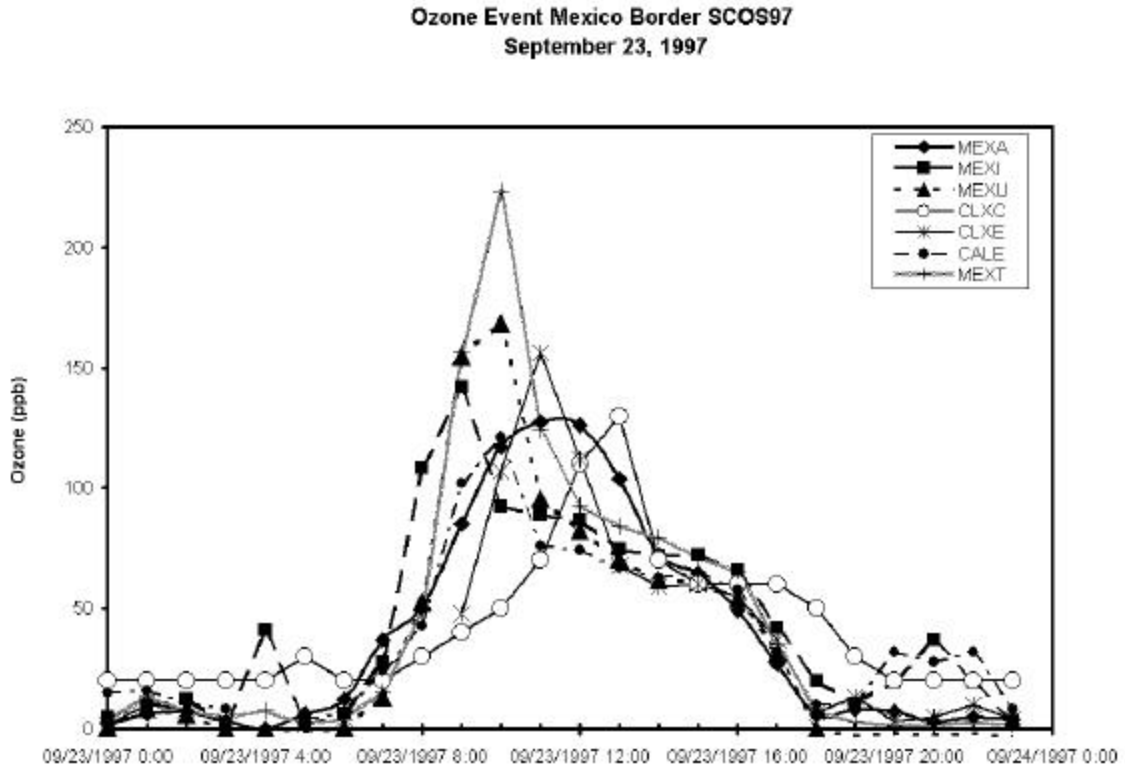


**Figure 10**. Hourly ozone concentrations at seven sites near the US-Mexico border on 23 September 1997. Concentrations begin to rise rapidly at 0800 PDT and reach peaks between 0900 and 1300 PDT.

Elsewhere in the region, ozone concentrations were not particularly high. However, elevated ozone concentrations were reported in Ventura County and an exceedance of the 1-hr ozone standard was reported in Santa Barbara County during this period. Ozone concentrations for intensive operational days during the episode are summarized in **Table 6**. On 22 September, the monitoring site at Simi Valley High School recorded a peak concentration of 101 ppb. On September 23, ozone concentrations reach 101 ppb at the Thousand Oaks monitor, 103 ppb at the West Casitas Pass monitor, and 137 ppb at the Capitan LFC #1 monitor.

**Table 6**. List of SCOS-97 Intensive Operational Days occurring between 21 - 24 September 1997 and observed Maximum Ozone concentrations.

| Date | Day | SCOS Episode Type | Maximum observed 1-hr/8-hr $O_3$ concentrations, ppb | | | | | | |
|---|---|---|---|---|---|---|---|---|---|
| | | | South Coast Air Basin | Ventura County | San Diego County | Mojave Desert | Santa Barbara County | Imperial County | Mexico |
| Sep 22 | Mon | No episode | 90/ 80 | 101/ 88 | 100/ 79 | 60/ 57 | 80/ 75 | 70/ 55 | 87/75 |
| Sep 23 | Tue | Eddy transport to Ventura following episode in South Coast Air Basin | 110/ 88 | 103/ 80 | 90/ 76 | 60/ 55 | 137/108 | 160/ 92 | 223/119 |

## 4.2 Meteorology

At the beginning of the four-day simulation episode, the synoptic-scale was dominated by a 500-mb ridge located just west of the CA coast with a moderately strong 571-dm cut-off low and trough located inland over eastern NV (**Figure 11**). The ridge and trough pattern produced a general northerly upper-level flow over most of CA at 0000 UTC (1700 PDT), 21 September, with sharply cyclonic winds in the bottom of the trough over the SoCAB and northern Baja CA. The upper-level trough was responsible for widespread low sea-level pressures over the Southwest U.S. with a 1002-mb low center in southern AZ (**Figure 12**). Skies were generally clear over CA and northern Baja at this time. A plot of the standard and special SCOS-97 surface data at 0000 UTC shows widespread mature sea-breeze winds over the SoCAB (**Figure 13**). Wind speeds are generally on the order of ~5 knots (~2.5 $ms^{-1}$). Temperatures observed in the LA Basin are ~23-27 C, with inland temperatures in the deserts as high as 31-37 C. Farther

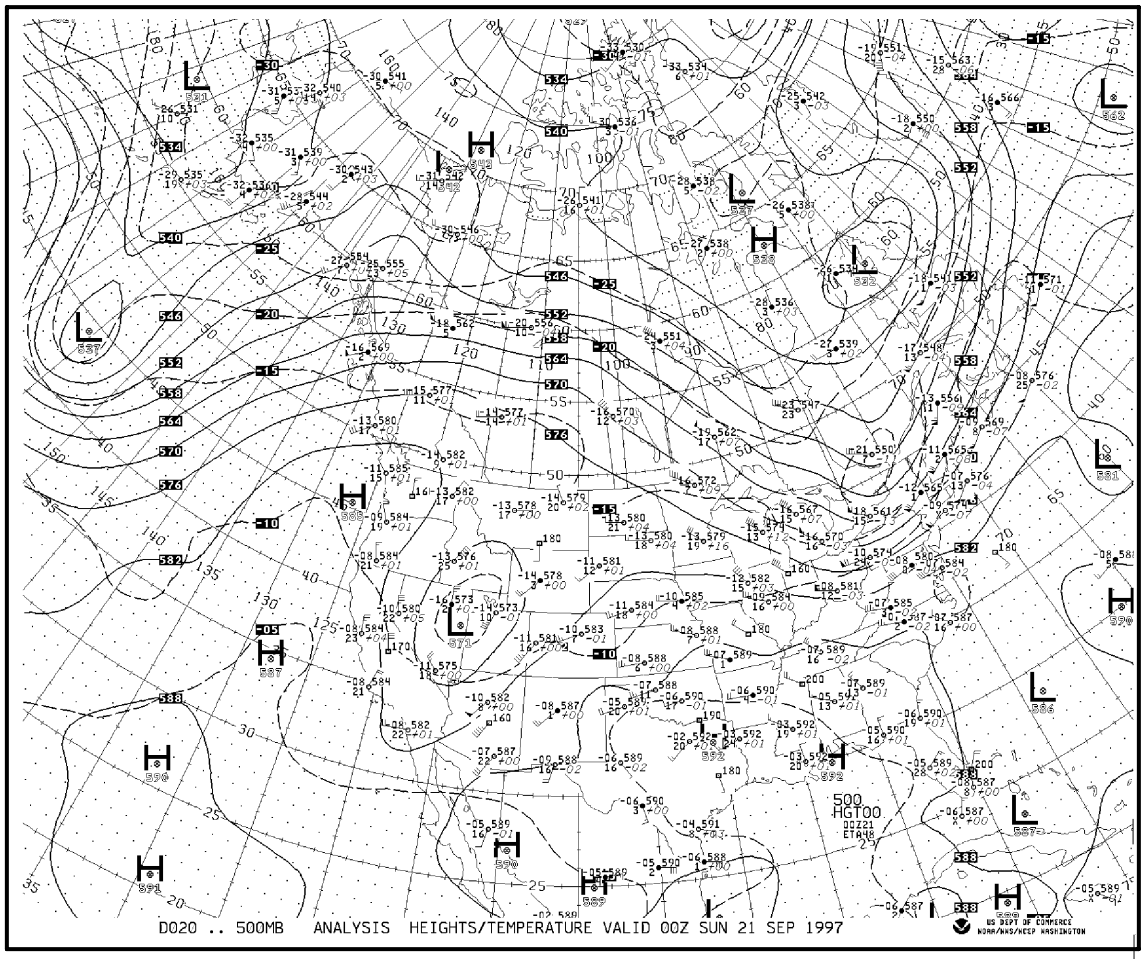


**Figure 11.** NCEP 500-mb analysis of geopotential heights (solid, dm) and temperature (C) at 0000 UTC, 21 September 1997. Contour interval is 6 dm. Isotherm interval is 5 C.

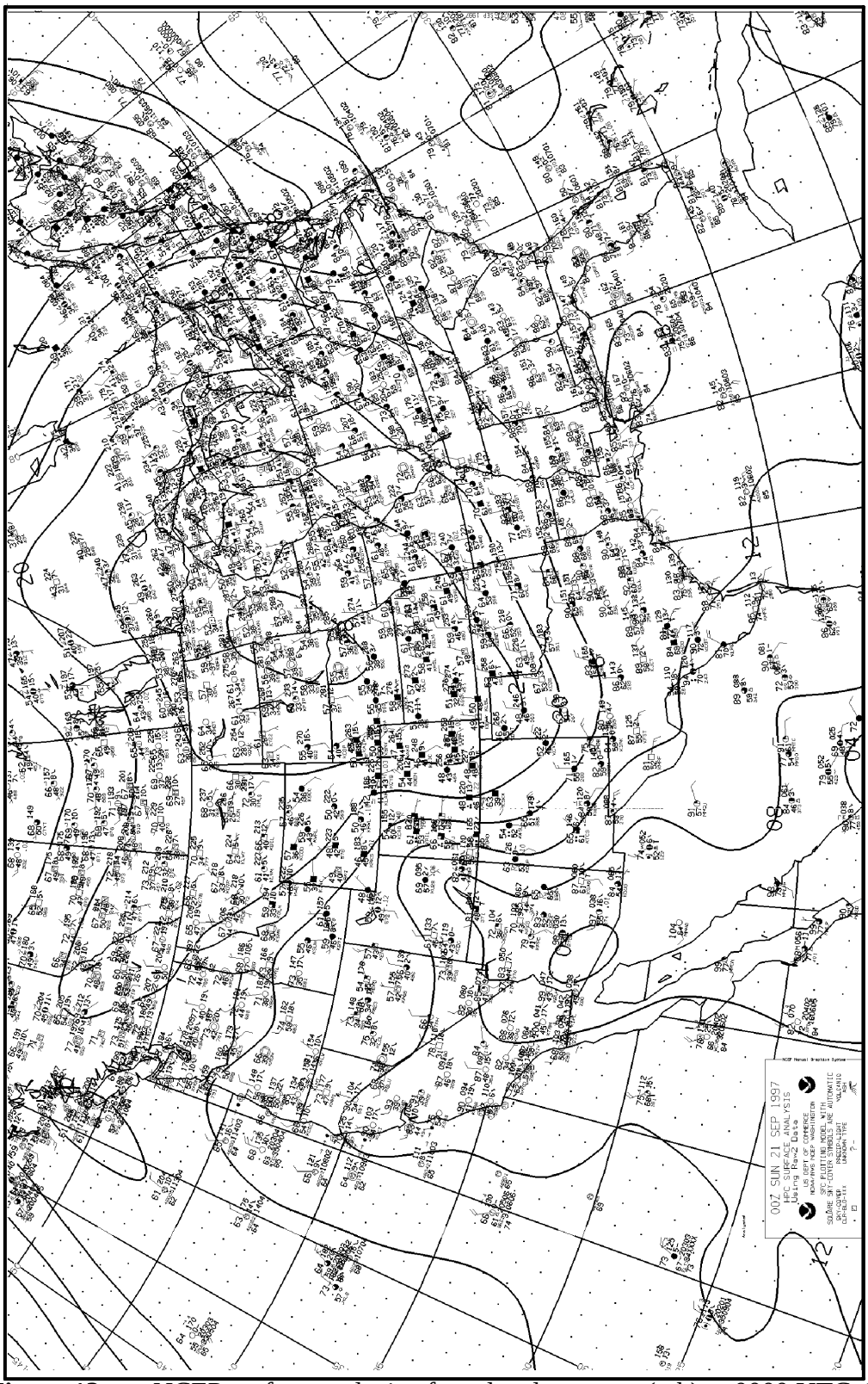


00/21

**Figure 12.** NCEP surface analysis of sea-level pressure (mb) at 0000 UTC, 21 September 1997. Contour interval is 4 mb.

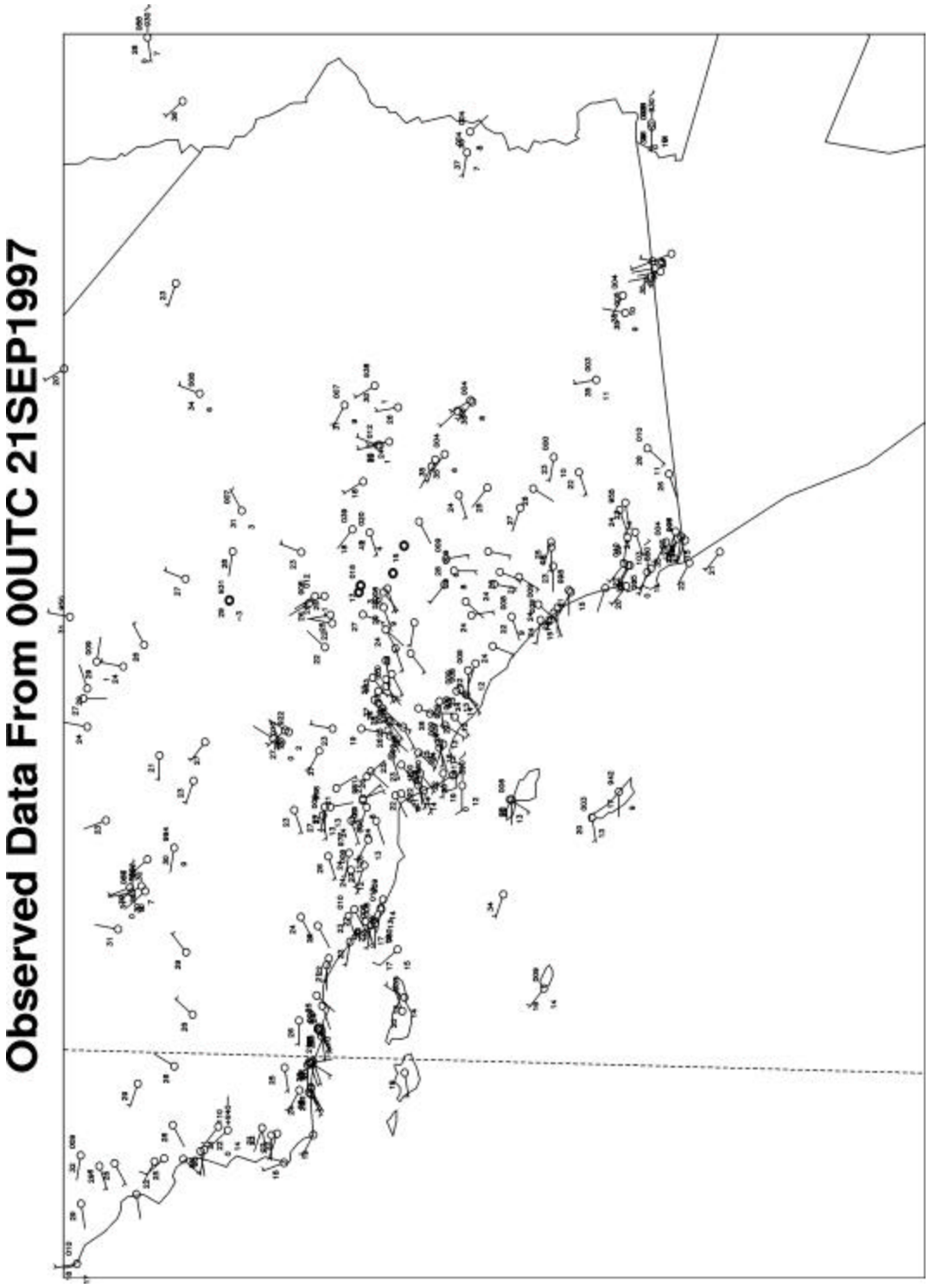


**Figure 13.** Plot showing standard NWS and special SCOS-97 surface observations at 0000 UTC, 21 September 1997. Wind is shown in knots (half barb = 5 kts, full barb = 10 kts). Temperatures and dew points are in degrees C.

inland and away from the influence of the sea breeze, wind directions are variable under the influence of local terrain (valley breezes), but generally have a northerly component in response to the mid-level and upper level forcing shown in **Figure 11**. The sea breeze is not as strong as commonly found during summer months because the land-sea thermal contrast is beginning to weaken by late September.

Over the following 3 h, the commencement of nocturnal cooling mostly eliminates the land-sea thermal contrast and the sea breeze rapidly weakens (not shown). By 0600 UTC (2300 PDT), 21 September, the winds in the SoCAB are mostly calm, with some weak downslope winds (mountain breezes) developing inland near the major terrain features (**Figure 14**). This gives a chaotic appearance to the inland winds, with no consistently favored direction at this time. Temperatures across the LA Basin at 0600 UTC are ~15-18 C, with a few sites reporting 20-21 C. The deserts of southeastern CA report temperatures of 24-29 C at this time. Just before sunrise, at 1200 UTC (0500 PDT), the land breeze and mountain breeze are at their greatest strength, as shown by the wind directions in **Figure 15**, but the wind speeds are very weak and many sites continue to show calm winds interspersed with the directed flow. This reveals the extremely localized and shallow nature of the land and mountain breezes, which presents a major challenge for a numerical model, even with a 5-km grid. Temperatures have continued to fall slowly through the latter part of the night, so that the LA Basin stations are reporting ~13- 18 C, with almost no sites at 20 C by 1200 UTC. In the deserts, temperatures are very mixed and range from ~10 C up to as high as 25 C.

By three hours later, at 1500 UTC (0800 PDT), the sun has risen but temperatures over land have not responded sufficiently to initiate a new sea breeze (not shown). Even at the coast, the land breeze still prevails at this time. However, by 1800 UTC (1100 PDT), the sea breeze and valley breeze has begun as temperatures in the LA Basin climb to ~25-29C (**Figure 16**). Inland, the dominant northerly component in the flow has returned as the PBL begins to deepen and mix momentum downward from the mid-levels to the surface. However, the wind speeds at this time remain rather light (mostly 1-3 $ms^{-1}$) and quite a few sites in the SoCAB are still reporting calm winds. Finally, by 2100 UTC (1400 PDT), the sea-breeze has matured again to 2-4 $ms^{-1}$ and northerly directions dominate the inland deserts through the afternoon, completing a diurnal cycle for the early part of the study period (not shown). Temperatures in the mid-afternoon peak at about 30-33 C in the LA Basin (cooler immediately along the coast), with maximums of 34-37 C at some desert locations (not shown).

Over the next 48 h the upper-level low noted at the beginning of the episode propagated slowly eastward and was located over Cheyenne WY by 0000 UTC, 23 September 2003 (**Figure 17**). This allowed the upper-level eastern Pacific ridge to propagate eastward over the CA coast, while weakening somewhat. The approach of an upper ridge over the SoCAB usually is accompanied by enhanced subsidence and it coincided with intensification of pollution concentrations. Under the influence of this upper-level regime the surface low-pressure system over the Southwest weakened by 0000 UTC, 23 September, leaving just a thermal trough over CA oriented from southeast to northwest **(Figure 18)**. In the SoCAB, the sea breeze appeared quite similar to other days, with westerly and northwesterly flow farther west over the CA Bight (**Figure 19**). However, to the east of the surface thermal trough, easterly to southeasterly winds had become established farther inland over the southern San Joaquin Valley and the desert

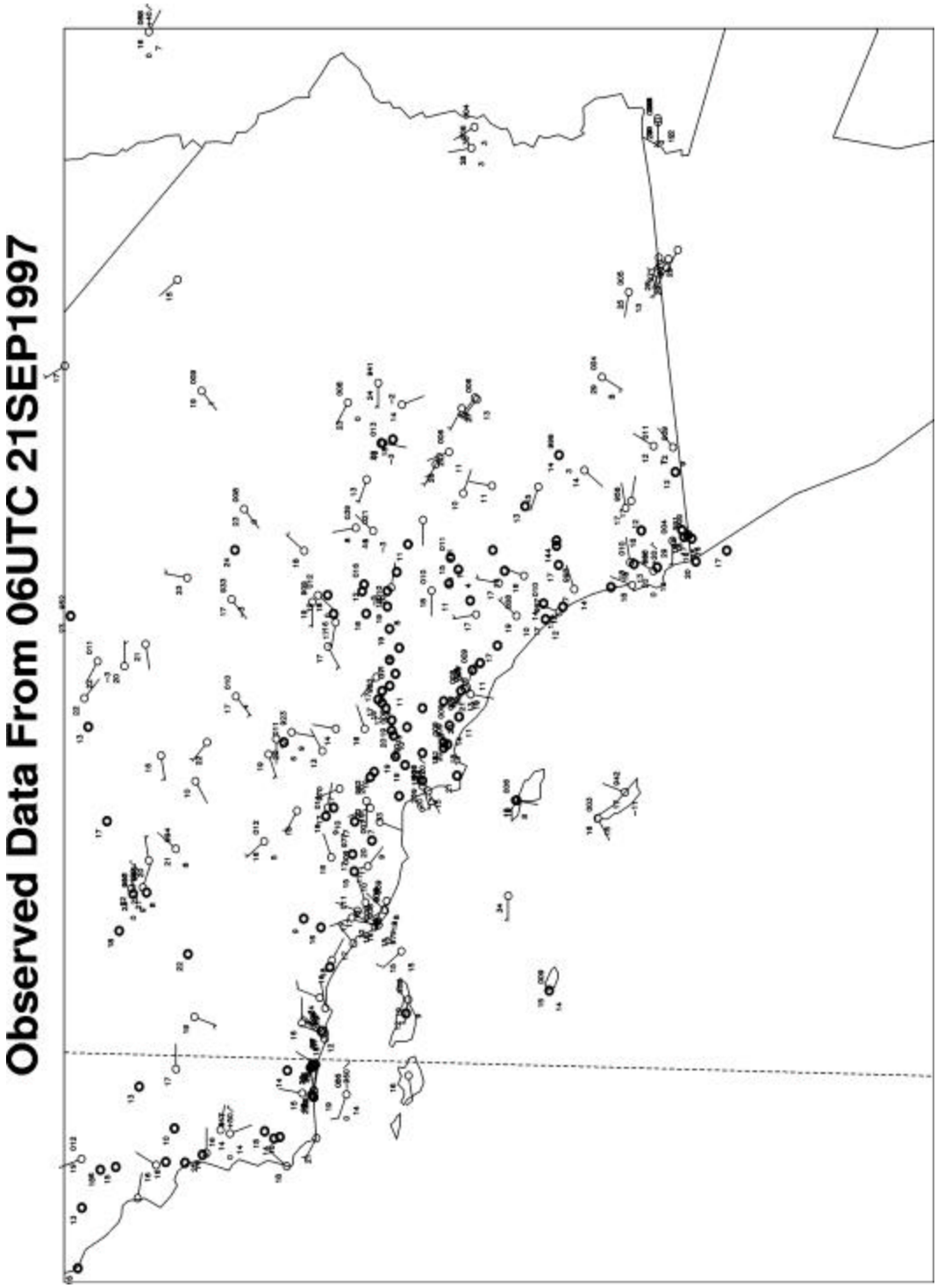


**Figure 14.** Plot showing standard NWS and special SCOS-97 surface observations at 0600 UTC, 21 September 1997. Wind is shown in knots (half barb = 5 kts, full barb = 10 kts). Temperatures and dew points are in degrees C.

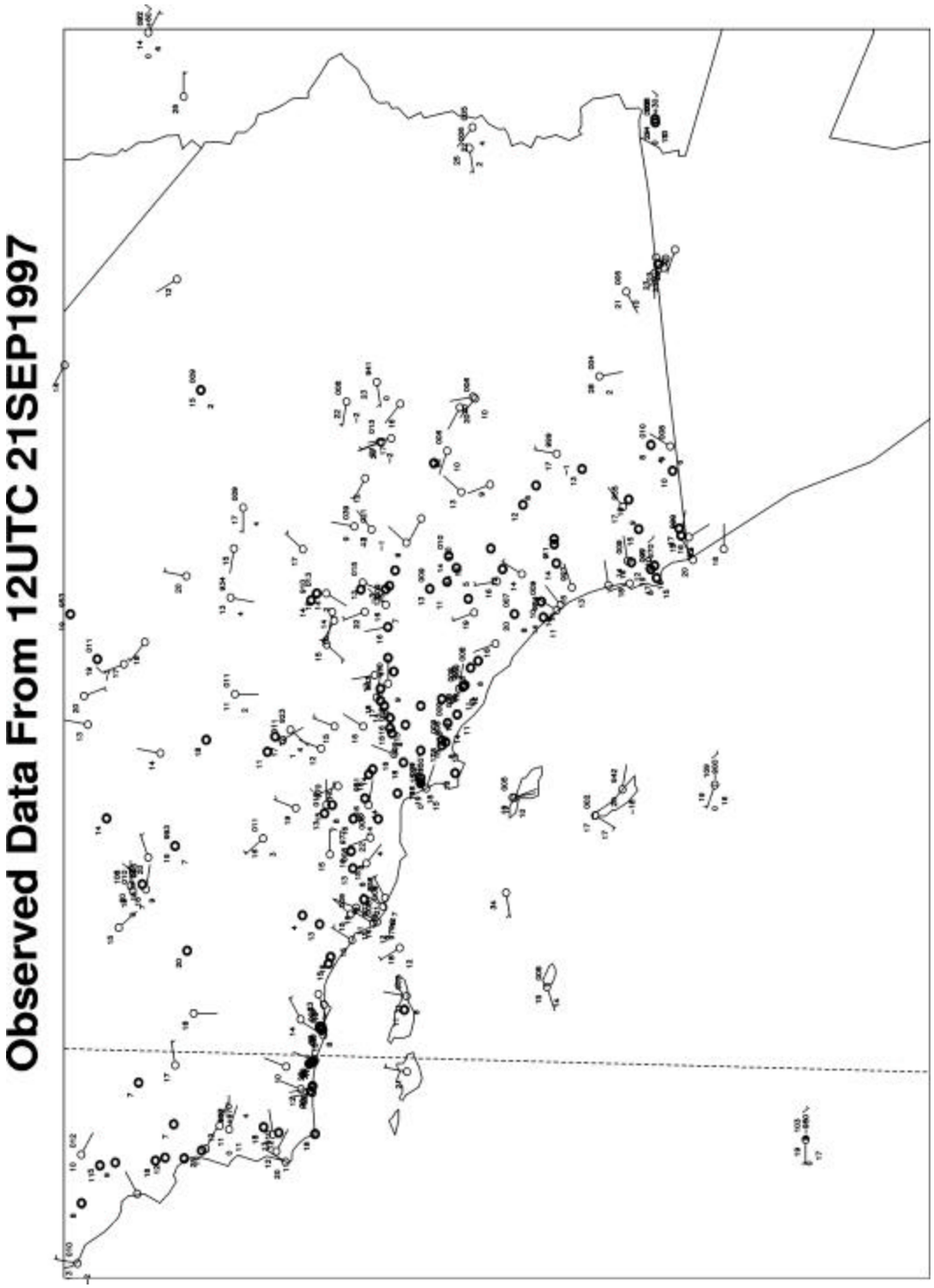


**Figure 15.** Plot showing standard NWS and special SCOS-97 surface observations at 1200 UTC, 21 September 1997. Wind is shown in knots (half barb = 5 kts, full barb = 10 kts). Temperatures and dew points are in degrees C.

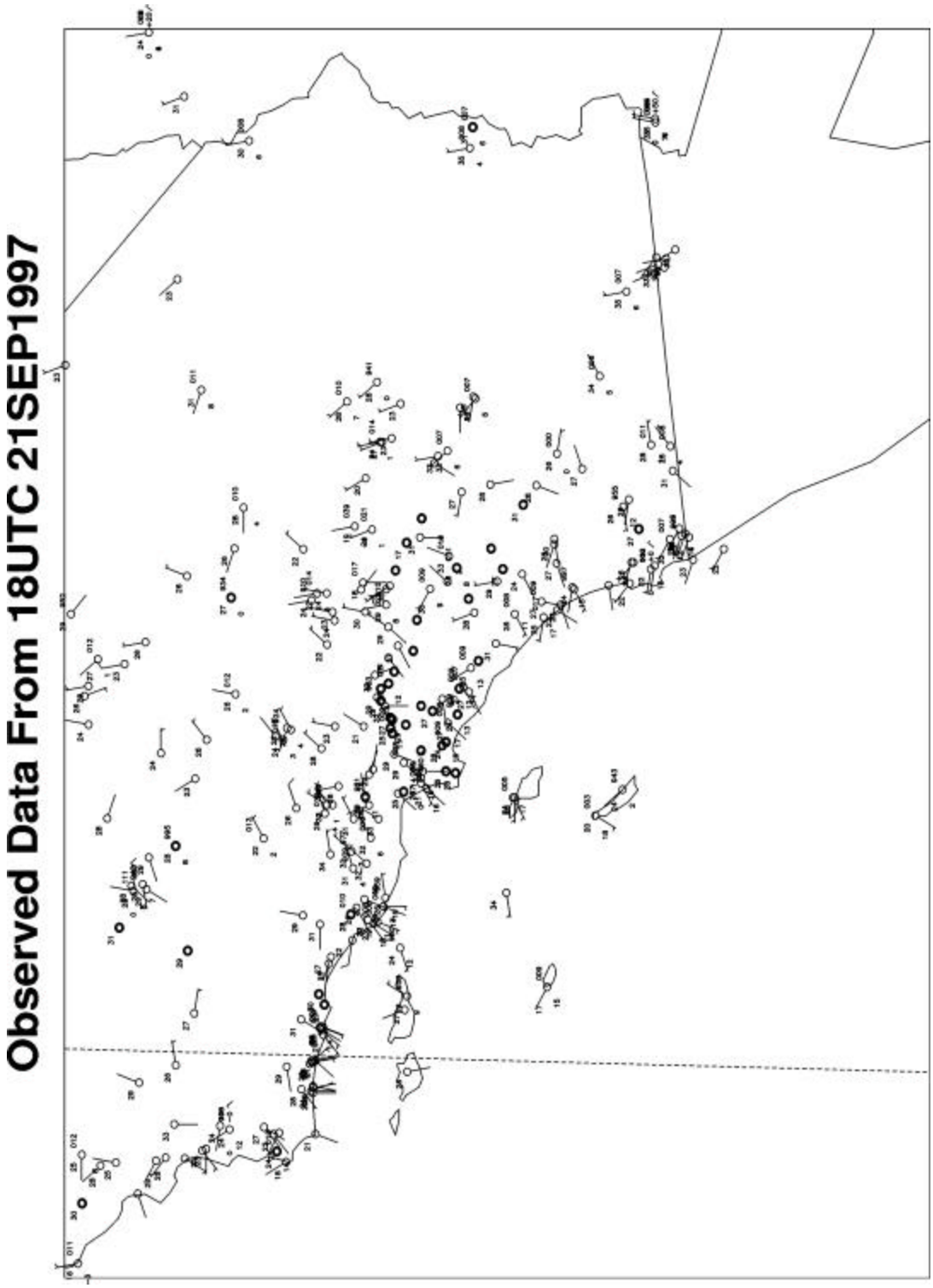


**Figure 16.** Plot showing standard NWS and special SCOS-97 surface observations at 1800 UTC, 21 September 1997. Wind is shown in knots (half barb = 5 kts, full barb = 10 kts). Temperatures and dew points are in degrees C.

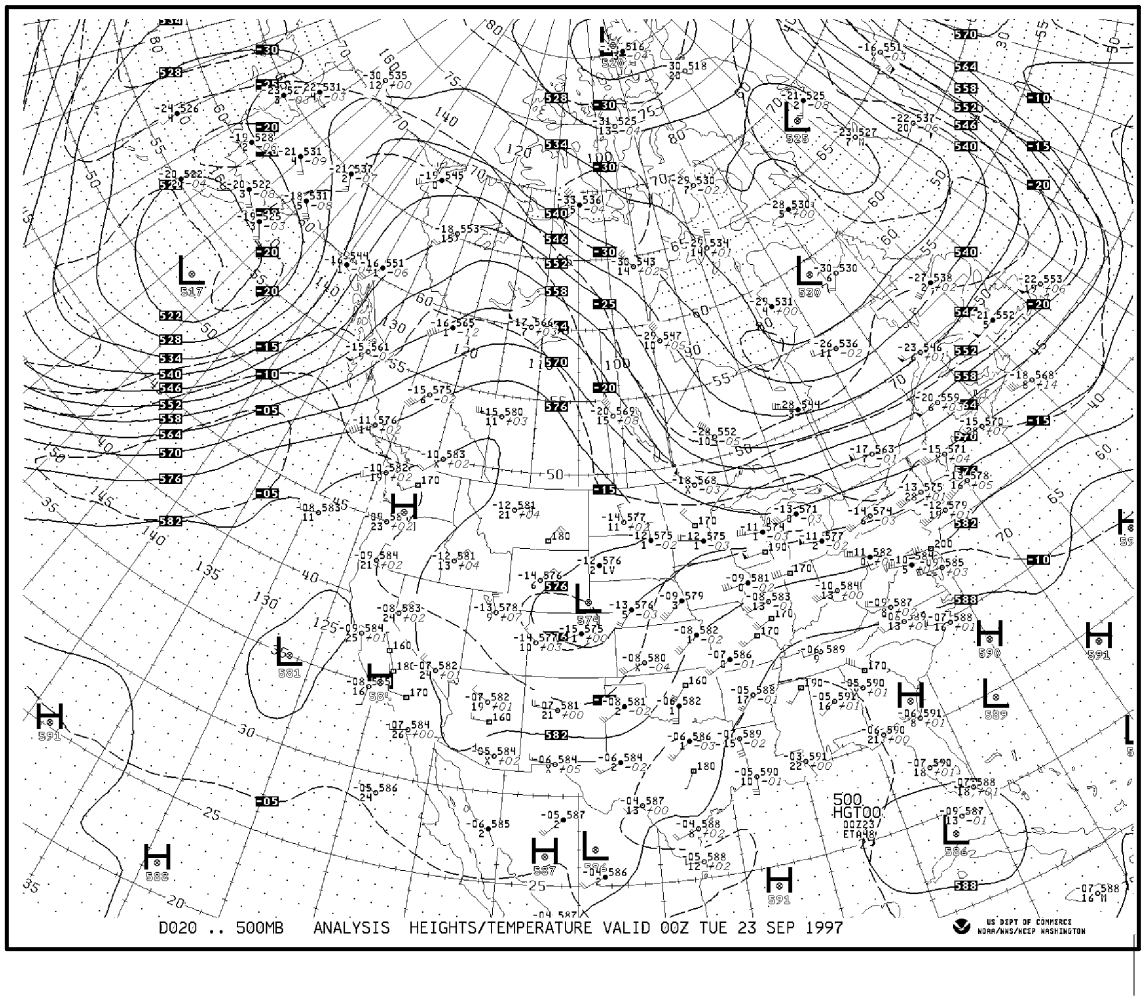


**Figure 17.** NCEP 500-mb analysis of geopotential heights (solid, dm) and temperature (C) at 0000 UTC, 23 September 1997. Contour interval is 6 dm. Isotherm interval is 5 C.

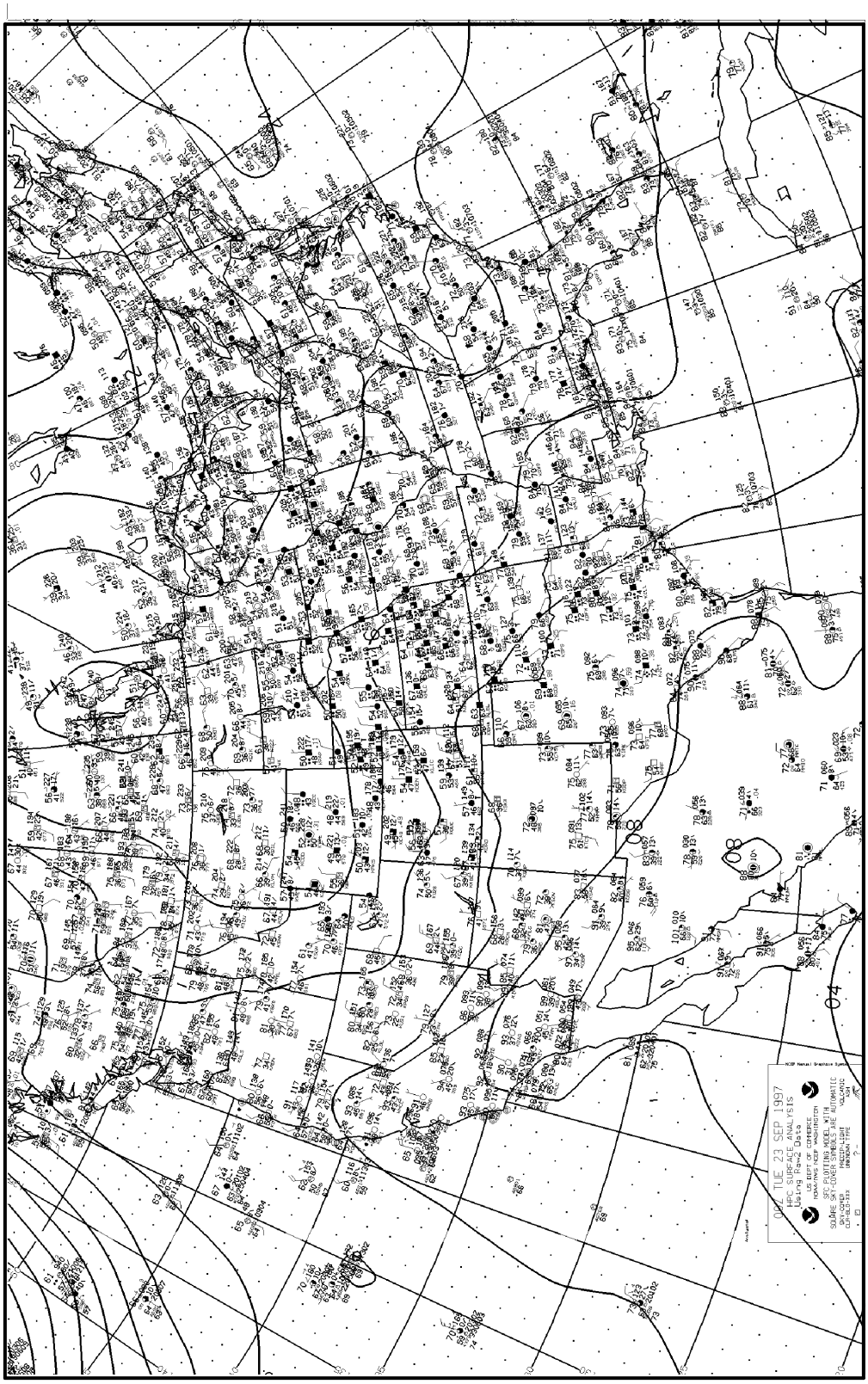


00/23

**Figure 18.** NCEP surface analysis of sea-level pressure (mb) at 0000 UTC, 23 September 1997. Contour interval is 4 mb.

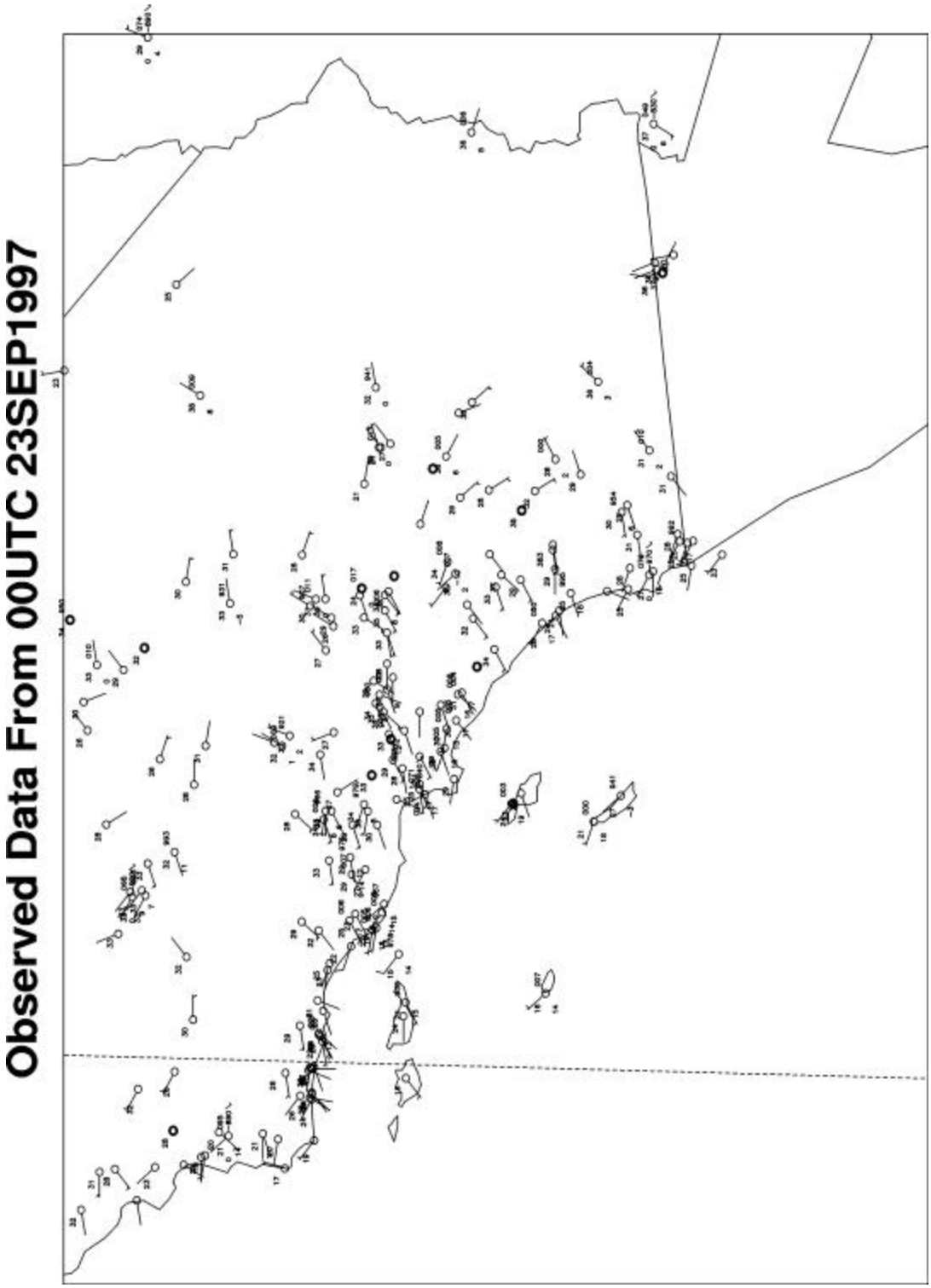


**Figure 19.** Plot showing standard NWS and special SCOS-97 surface observations at 0000 UTC, 23 September 1997. Wind is shown in knots (half barb = 5 kts, full barb = 10 kts). Temperatures and dew points are in degrees C.

regions of southeastern CA. Much farther south, beyond the tip of the Baja Peninsula, a tropical cyclone had formed and was beginning to move northward by 0000 UTC, 23 September (not shown). That cyclone was already spreading clouds over southern Baja and parts of western Mexico, along with a few showers and drizzle (**Figure 18**). The circulation about this system would have an increasing influence on the SoCAB over the remainder of the episode.

Through the next day, 23 September, the tropical cyclone gradually moved northward to the southern end of Baja. The 500-mb ridge had become well established over the Rocky Mountains by 0000 UTC, 24 September (**Figure 20**), with its axis from eastern BC to central AZ. The 500-mb flow over the SoCAB was light and had a mostly southerly component. This can be a generally favorable configuration for air stagnation conditions. By this time the approach of the tropical cyclone was beginning to affect surface conditions over the SoCAB, so that the normally persistent surface thermal trough had become rather weak (not shown). Meanwhile, the coastal sea-breeze winds at 0000 UTC, 24 September, were lighter than normal (~2-3 kts) and the inland winds became east and southeasterly under the influence of the tropical cyclone circulation (**Figure 21**). The weakening of the sea breeze led to warming of temperatures across the SoCAB by 1-5 C.

The effect of the slowly intensifying easterlies aloft (not shown), in response to the approaching cyclone, can be seen in the surface data at 1200 UTC, 24 September (**Figure 22**). At this time the easterly component of the land breeze is somewhat reinforced by the growing cyclonic circulation around the tropical storm and surface temperatures are 2-6 C warmer in the SoCAB than at 1200 UTC, 21 September (**Figure 15**). During the morning hours following sunrise temperatures again rose over the region, but the circulation of the tropical cyclone opposed the formation of the normal sea breeze. **Figure 23** shows general easterly flow across all of southern CA at 1800 UTC, 24 September, with westerly components mostly isolated along the immediate coastline. At the same time, the tropical cyclone can be seen moving northward off the western coast of Baja CA in a visual GOES satellite image, with its cloud shield extending approximately to the Mexican border **(Figure 24)**. By the end of the study period at 0000 UTC, 25 September, a surface trough runs eastward from the LA Basin to southern NM and marks the advance of moist tropical air into the SoCAB **(Figure 25)**. Local SCOS observations revealed mostly southeasterly winds below the trough at that time (**Figure 26**), accompanied by some rain showers (**Figures 25 and 26**).

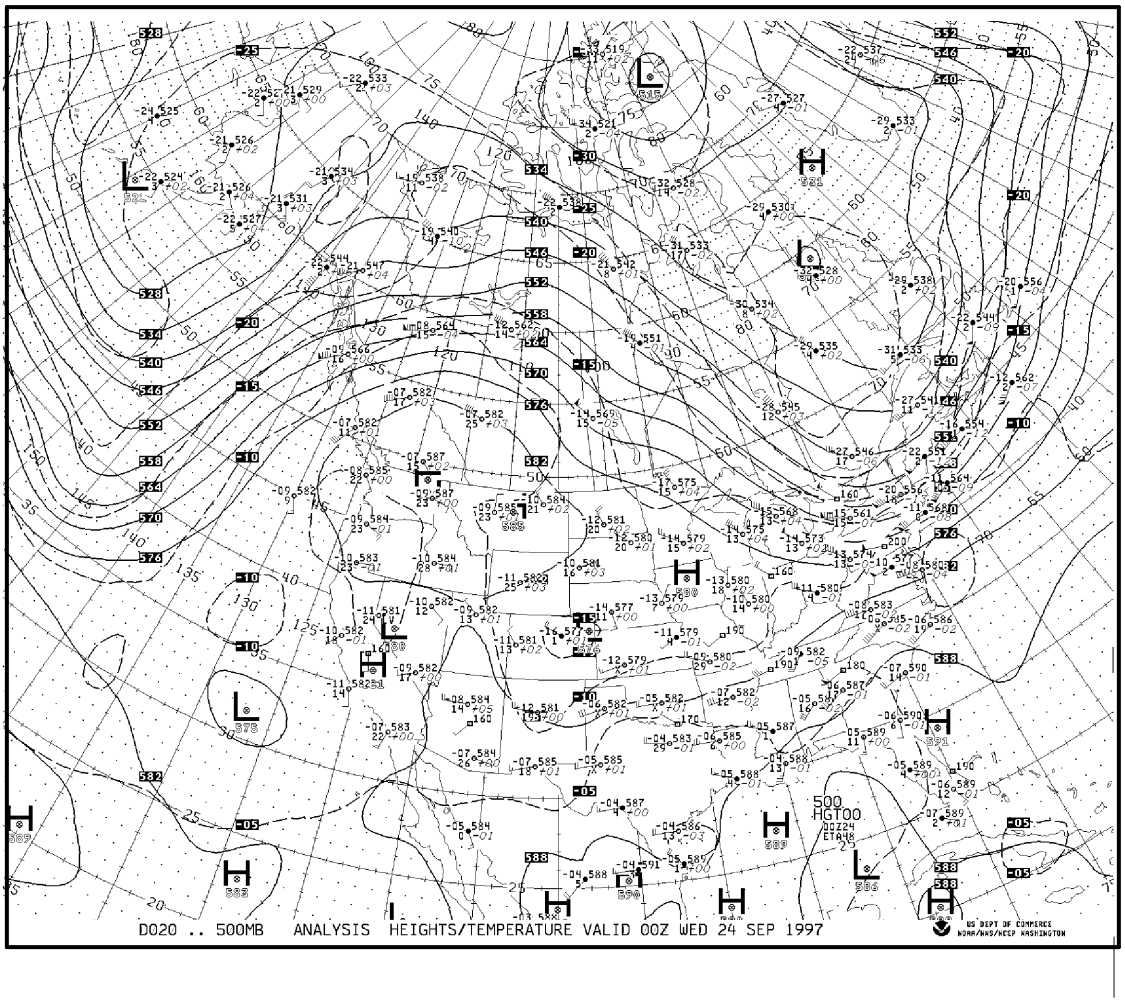


**Figure 20.** NCEP 500-mb analysis of geopotential heights (solid, dm) and temperature (C) at 0000 UTC, 24 September 1997. Contour interval is 6 dm. Isotherm interval is 5 C.

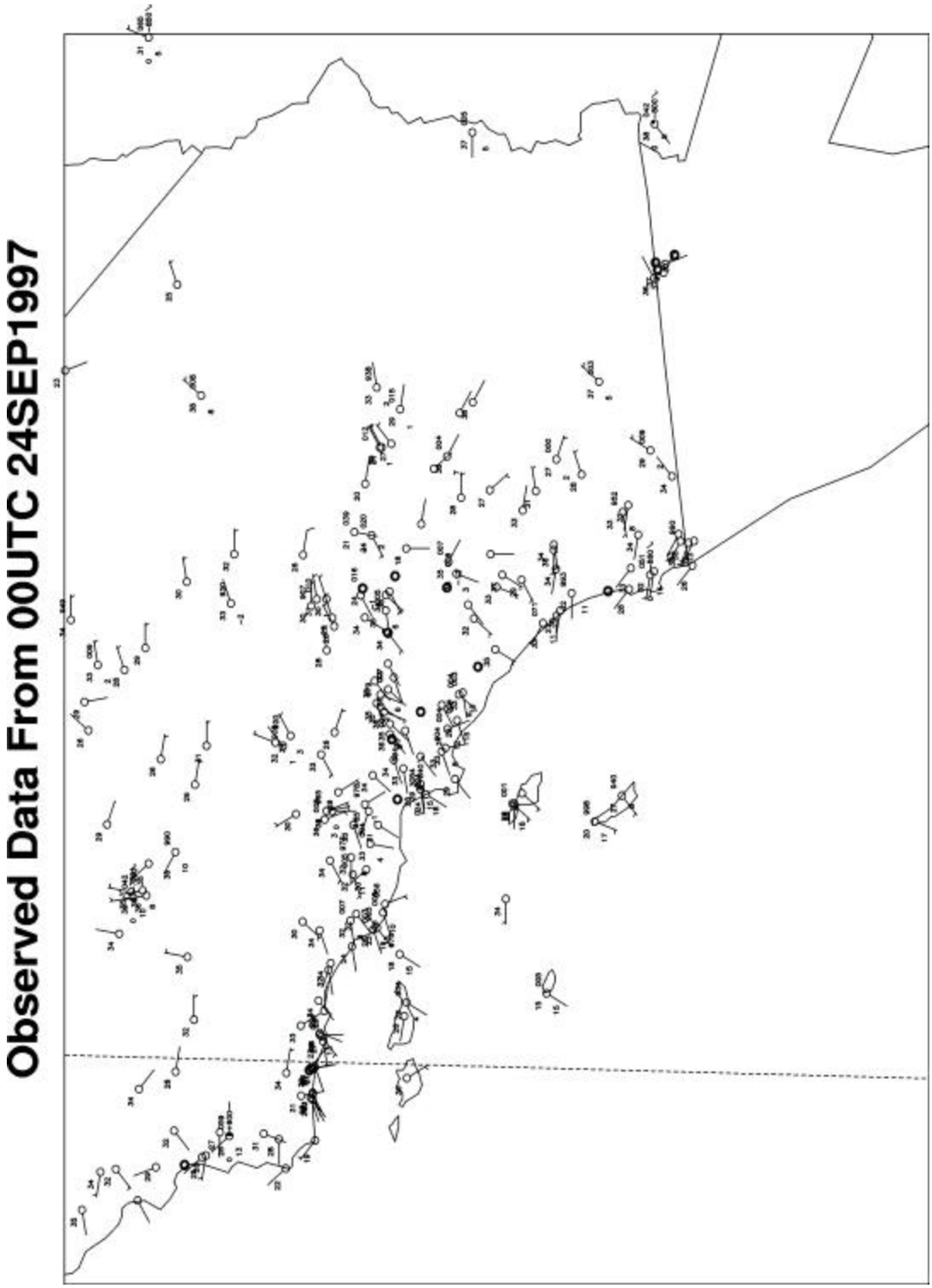


**Figure 21.** Plot showing standard NWS and special SCOS-97 surface observations at 0000 UTC, 24 September 1997. Wind is shown in knots (half barb = 5 kts, full barb = 10 kts). Temperatures and dew points are in degrees C.

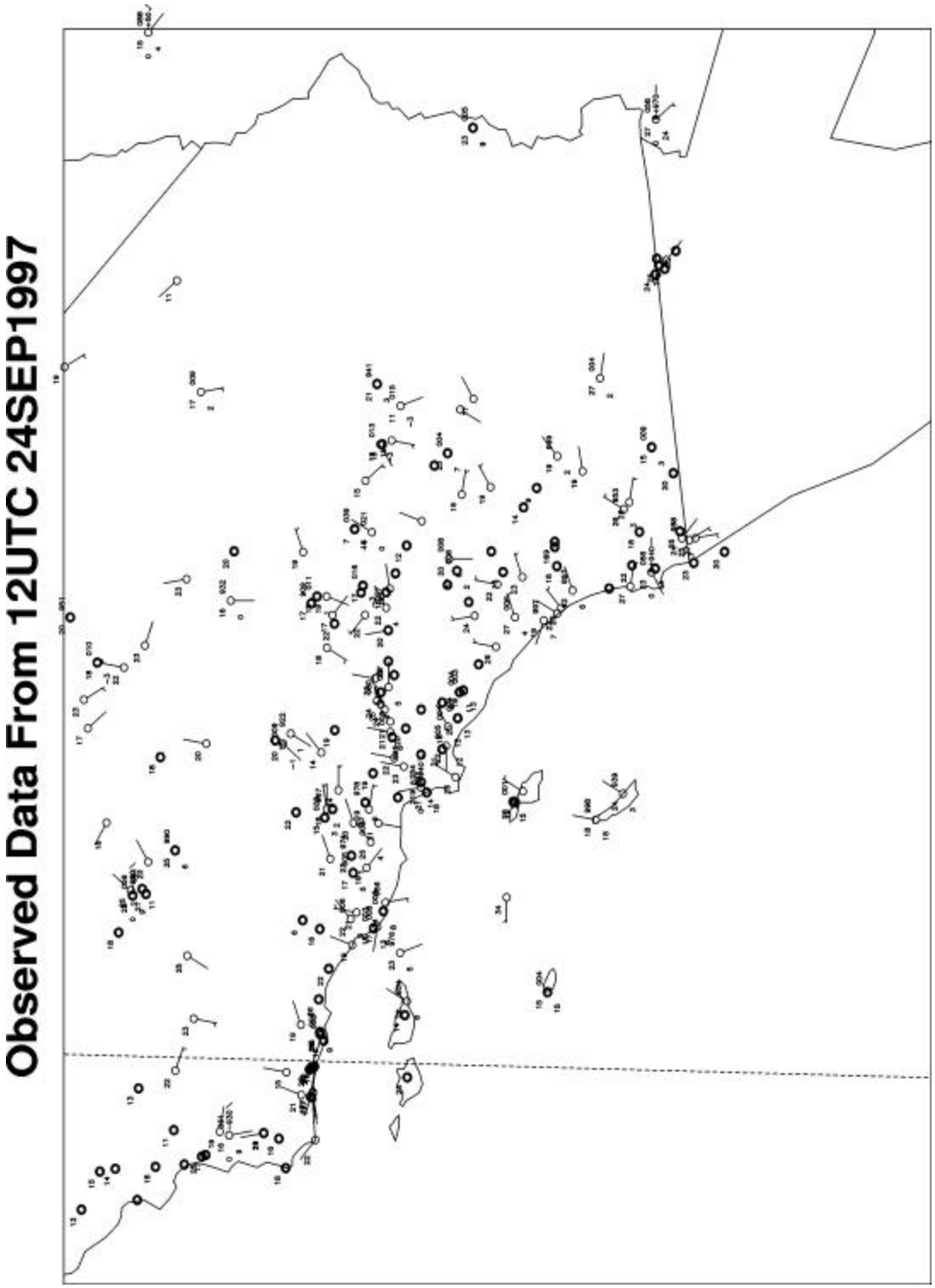


**Figure 22.** Plot showing standard NWS and special SCOS-97 surface observations at 1200 UTC, 24 September 1997. Wind is shown in knots (half barb = 5 kts, full barb = 10 kts). Temperatures and dew points are in degrees C.

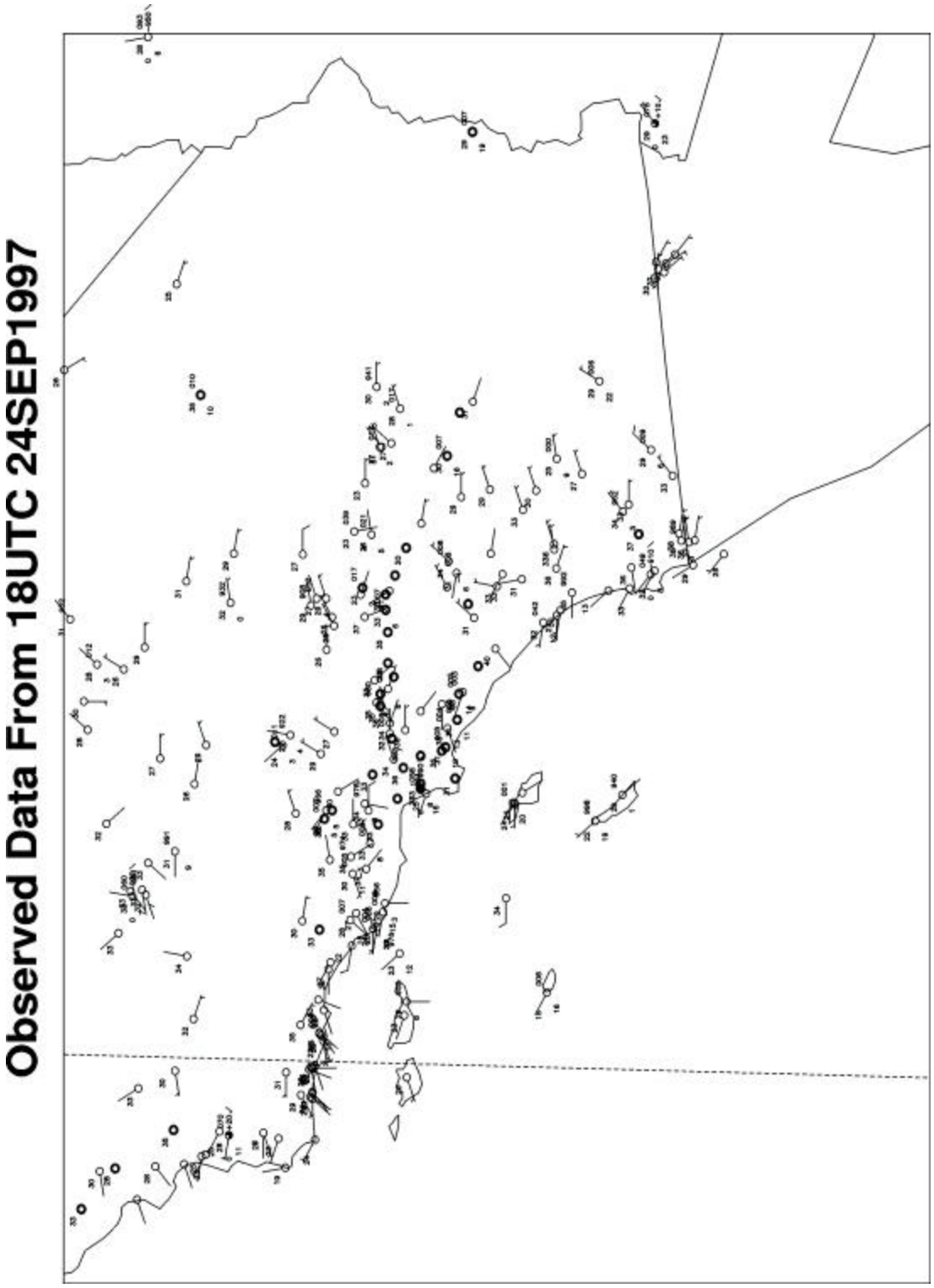


**Figure 23.** Plot showing standard NWS and special SCOS-97 surface observations at 1800 UTC, 24 September 1997. Wind is shown in knots (half barb = 5 kts, full barb = 10 kts). Temperatures and dew points are in degrees C.

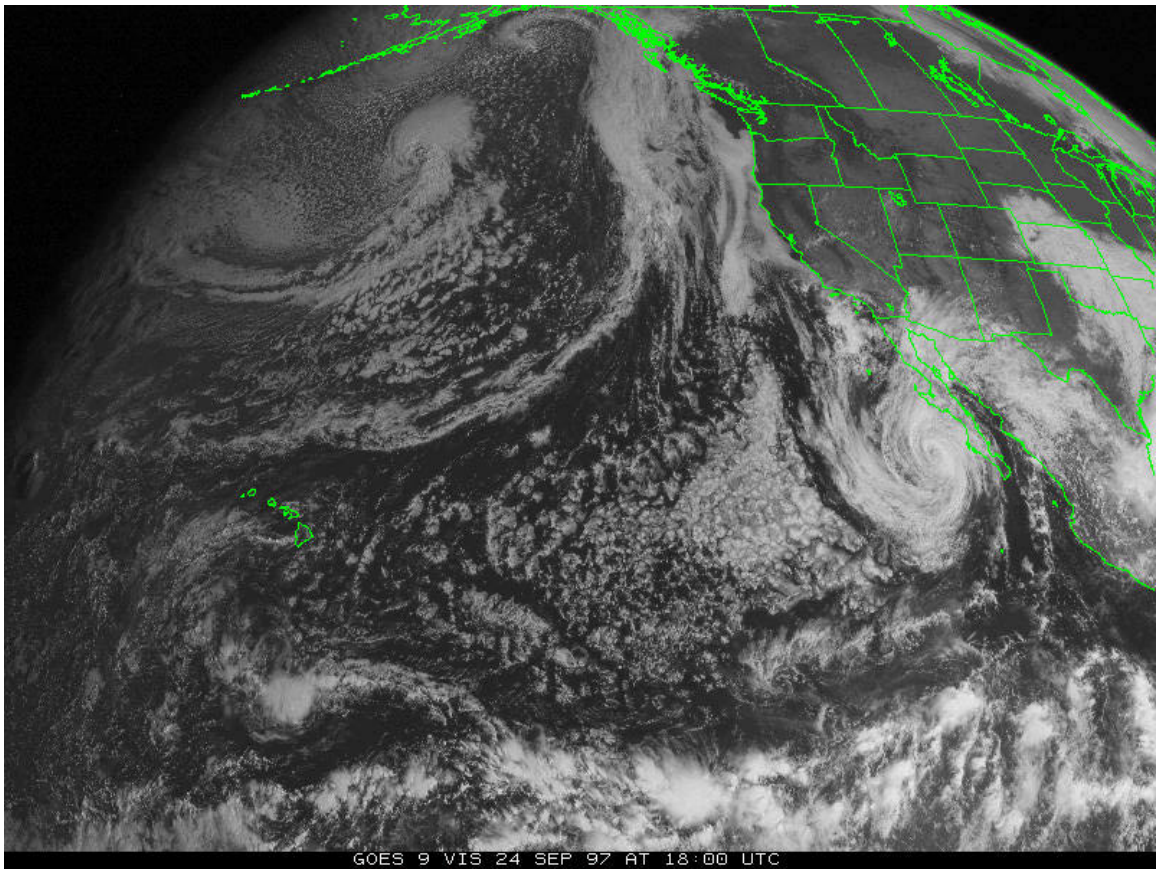


**Figure 24.** GOES 9 visible image from 1800 UTC, 24 September 1997.

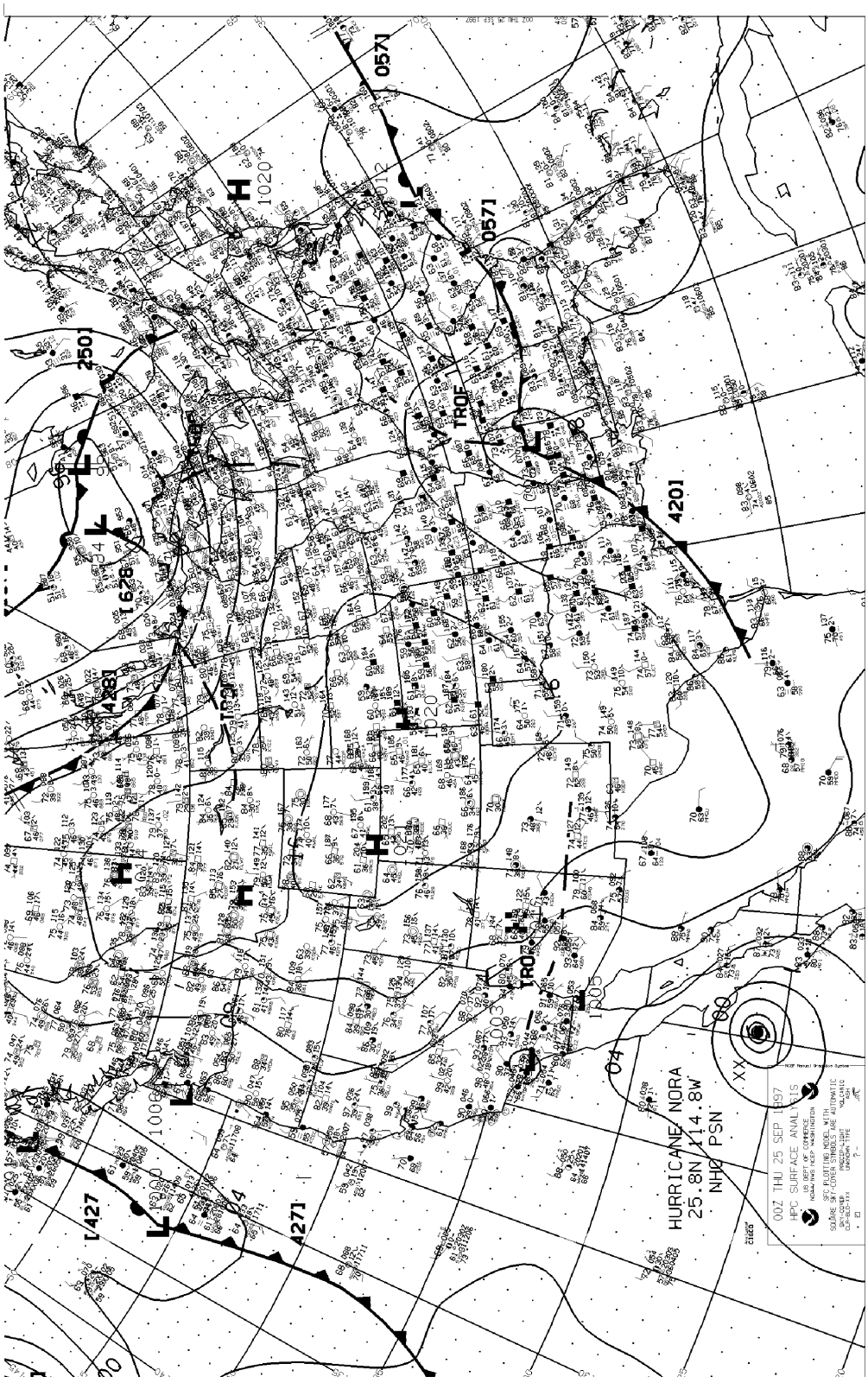


**Figure 25.** NCEP surface analysis of sea-level pressure (mb) at 0000 UTC, 25 September 1997. Contour interval is 4 mb.

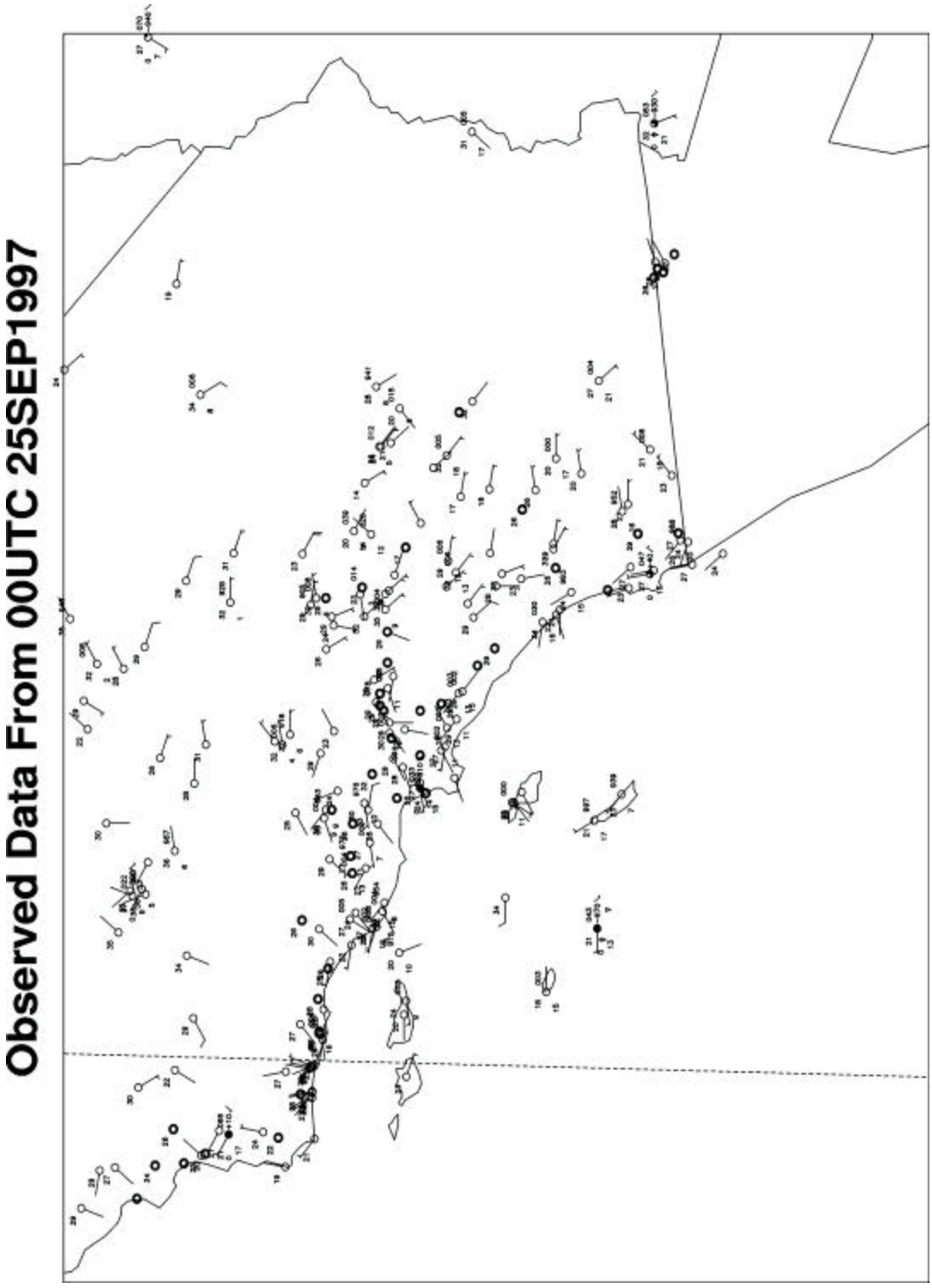


**Figure 26.** Plot showing standard NWS and special SCOS-97 surface observations at 0000 UTC, 25 September 1997. Wind is shown in knots (half barb = 5 kts, full barb = 10 kts). Temperatures and dew points are in degrees C.

## 4.3 Conceptual Model

Before any simulations were undertaken, STI reviewed both the meteorological and air quality conditions during the episode to develop a conceptual model of the ozone formation, transport, and diffusion processes. STI reviewed analyses of meteorological data, inspected emission density plots of the region, identified the locations of peak ozone concentrations, and prepared contour maps of ozone and ozone precursors. The goal of these analyses was to identify source-receptor relationships, critical transport pathways, and distinct meteorological features (i.e., convergence zones, land/sea breezes, slope flows, and mixing layer evolution) that would be used in the model performance evaluation.

While this episode did include SCOS-97 intensive operating days (22 and 23 September), additional upper-air observations were not available for developing our conceptual model. Also, all RWP data at El Centro was invalidated for this period. Further, Mexican meteorological and air quality data were limited to sites along the border and there are likely to be many emission sources in Mexico that are not in the SCOS-97 inventory. Despite these limitations, we have developed a conceptual model that can, at least partially, explain the ozone events that occurred during this period.

The key meteorological features responsible for elevated ozone concentrations along the border and in Ventura and Santa Barbara counties were the passage of the upper-level ridge on 22 September, followed by the approach of the tropical cyclone that was moving northward off the western coast of Baja CA. **Figure 27** shows a time-series analysis of meteorology and air quality at the Collegio de Bachilleres -Mexicali (MEXA) monitoring site, which is useful in explaining the evolution of the episode. Early in the period (19 and 20 September) wind flow over the region was northwesterly with ozone and ozone precursors transported southeastward from the South Coast Air Basin (SoCAB) into the deserts. However, as the upper ridge began to weaken, the winds became lighter (21 September) allowing some local accumulation of ozone and ozone precursors. The presence of ozone aloft at the border is indicated by the rapid ozone increases seen at the MEXA site on the morning of 21 September. By the afternoon of September 22 the winds became light and predominately southeasterly, allowing ozone and ozone precursors to be transported from the SoCAB into Ventura County and from northern Mexico into Mexicali.

On 23 September the winds are light and the transported ozone and ozone precursors combine with local emissions (note the high NO concentrations at MEXA) resulting in rapid ozone formation in the border region between 0800 and 1300 PDT as the ozone plume moves northward. In Santa Barbara a similar combination of transport and local emissions is indicated, but ozone formation is not as rapid or early. At the Capitan LFC #1 site, an enhanced ozone peak of 126 ppb is seen at 1400 PDT, with a separate transport dominated peak occurring at 2200 PDT.

The cause of rapid ozone formation at sites in Mexicali and Calexico on 23 September is not completely clear. Normally, ozone production downwind of a significant emissions area continues throughout the day and concentration peaks are observed in the afternoon hours. Also,

the ozone scavenging by NO usually results in the ozone peak being downwind of the emission area. In this episode, the early ozone peak may be a result of ozone mixing down from aloft, highly reactive local emissions, or a combination of both. Early increases in ozone were seen on 21 and 22 September, which we believe are a result of mixing air down from aloft because the ozone peaks are correlated with wind speed increases. However, on 23 September the wind are light and the correlation is not clear. This implies that the reactivity of the local emissions may have been an important contributor. It could be that local emissions to the south of the monitors are sufficiently reactive to result in rapid ozone formation and only on days with southerly flow do we see these phenomena. An alternative explanation is also possible: that upset emissions were released during this period. Recent studies in Texas suggest that many industrial facilities experience upset conditions where highly reactive hydrocarbon emissions are emitted at levels many times higher than under normal operations. In Texas these upset emissions have been used to explain rapid ozone formation events in $NO_x$ rich areas.

Later, on 24 September the northward progress of the tropical storm caused winds across the entire region to increase dramatically. Strong advection from the east-southeast over the SoCAB led to strong ventilation, so that the time series in **Figure 27** indicates very clean air on this final day of the episode.

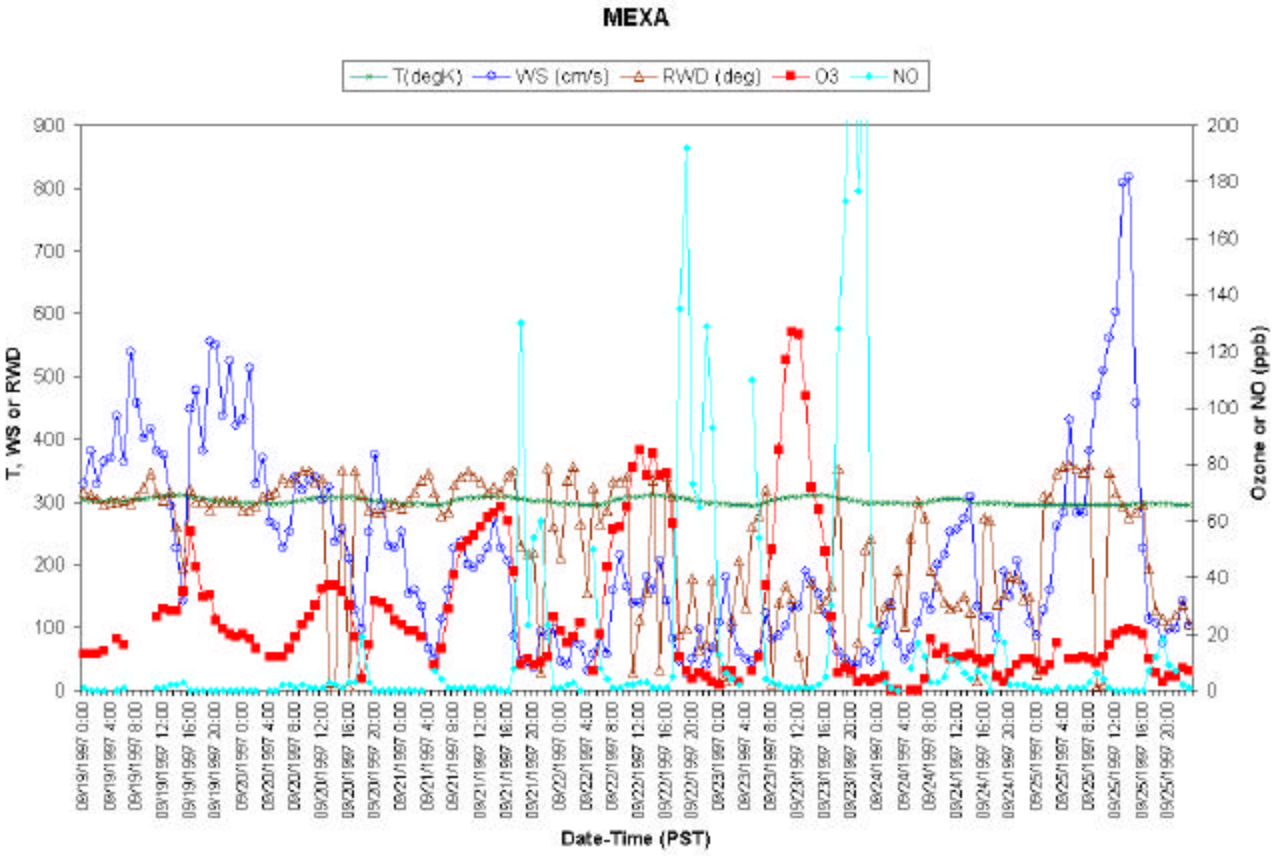


**Figure 27**. Time-series analysis of meteorology and air quality at the Collegio de Bachilleres -Mexicali (MEXA) monitoring site.